Conserved cysteine residues in Kaposi's sarcoma herpesvirus ORF34 are necessary for viral production and viral pre-initiation complex formation.

Tadashi Watanabe[1,*], Aidan McGraw[2], Kedhar Narayan[2], Hasset Tibebe[2], Kazushi Kuriyama[1], Mayu Nishimura[4], Taisuke Izumi[2,3], Masahiro Fujimuro[4], and Shinji Ohno[1,*]

1: Department of Virology, Graduate School of Medicine, University of the Ryukyus, 207 Uehara, Nishihara, Nakagami, Okinawa, 903-0215, Japan

2: Department of Biology, College of Arts & Sciences, American University, Washington, D.C., 20016, U.S.A.

3: District of Columbia Center for AIDS Research, Washington D.C., 20052, U.S.A.

4: Department of Cell Biology, Kyoto Pharmaceutical University, 1 Misasagi-Shichono, Yamashina, Kyoto 607-8412, Japan.

*: Address correspondence to Tadashi Watanabe, Ph.D. and Shinji Ohno, M.D, Ph.D., Department of Virology, Graduate School of Medicine, University of the Ryukyus, 207 Uehara, Nishihara, Nakagami, Okinawa, 903-0215, Japan; Tel: +81-98-895-1131 and +81-98-895-1708

E-mail: T.W.; twatanab@med.u-ryukyu.ac.jp, S.O.; soono@med.u-ryukyu.ac.jp

Running title: Profiling of the conserved residues in KSHV ORF34

ABSTRACT

Kaposi's sarcoma herpesvirus (KSHV) ORF34 plays a significant role as a component of the viral pre-initiation complex (vPIC), which is indispensable for late gene expression across beta and gamma herpesviruses. Although the key role of ORF34 within the vPIC and its function as a hub protein have been recognized, further clarification regarding its specific contribution to vPIC functionality and interactions with other components is required. This study employed a deep-learning algorithm-assisted structural model of ORF34, revealing highly conserved amino acid residues across human beta- and gamma-herpesviruses localized in structured domains. Thus, we engineered ORF34 alanine-scanning mutants by substituting conserved residues with alanine. These mutants were evaluated for their ability to interact with other vPIC factors and restore viral production in cells harboring the ORF34-deficient KSHV-BAC. Our experimental results highlight the crucial role of the 4 cysteine residues conserved in ORF34: a tetrahedral arrangement consisting of a pair of C-X_n-C consensus motifs. This suggests the potential incorporation of metal cations in interacting with ORF24 and ORF66 vPIC components, facilitating late gene transcription, and promoting overall virus production by capturing metal cations. In summary, our findings underline the essential role of conserved cysteines in KSHV ORF34 for effective vPIC assembly and viral replication, thereby enhancing our understanding of the complex interplay between the vPIC components.

42 **IMPORTANCE**

43 The initiation of late gene transcription is universally conserved across the gamma- and beta-
44 herpesvirus families. This process employs a viral pre-initiation complex (vPIC), which is
45 analogous to a cellular PIC. Although KSHV ORF34 is a critical factor for viral replication and
46 is a component of the vPIC, the specifics of vPIC formation and the essential domains crucial
47 for its function remain unclear. Structural predictions suggest that the 4 conserved cysteines
48 (C170, C175, C256, and C259) form a tetrahedron that coordinates the metal cation. We further
49 investigated the role of these conserved amino acids in interactions with other vPIC
50 components, late gene expression, and virus production, to demonstrate for the first time that
51 these cysteines are pivotal for these functions. This discovery not only deepens our
52 comprehensive understanding of ORF34 and vPIC dynamics but also lays the groundwork for
53 more detailed studies on herpesvirus replication mechanisms in future research.

54 **Introduction**

55 Human herpesviruses are classified into the *Alpha*-, *beta*-, and *Gamma-herpesvirinae*
56 subfamilies (1, 2). Kaposi's sarcoma herpesvirus (KSHV), also referred to as human
57 gammaherpesvirus-8 (HuGHV8) or human herpesvirus-8 (HHV-8), along with Epstein-Barr
58 virus (EBV), belongs to the *Gammaherpesvirinae* subfamily (1-3). Unique among human
59 herpesviruses, these human gamma herpesviruses possess direct pathogenicity toward
60 malignant neoplasms (3-5). KSHV plays a notable role in the pathogenicity of epithelial
61 malignancies with Kaposi's sarcoma (KS), and of B-lymphocyte malignancies with
62 multicentric Castleman's disease (MCD) and primary effusion lymphoma (PEL) (4, 6-9).
63 Additionally, KSHV infection can lead to an inflammatory disorder known as KSHV
64 inflammatory cytokine syndrome (KICS) (6-8).

65 The KSHV genome encodes more than 90 gene products, including proteins and
66 functional RNAs such as lncRNAs, miRNAs, and circRNAs (6, 10-14). The majority of these
67 genes are crucial for the KSHV life cycle, which incorporates 2 distinct phases: latent and lytic.
68 After primary infection, KSHV initially expresses a few genes known as latent genes, which
69 contribute to establishing and maintaining latency within infected cells (15). The transition
70 from a latent to lytic infection state necessitates certain reactivation stimuli to infected cells,
71 such as extracellular environmental changes and intracellular signaling alterations that result
72 in the upregulation of a multitude of KSHV-coding genes, referred to as lytic genes (16-18). In
73 association with the progress of virus-producing infection, the expression pattern of lytic genes
74 is divided into 3 sequential steps, resulting in the classification of lytic genes into immediate-
75 early (IE), early (E), and late (L) genes (6, 19, 20). The initial response to reactivation stimuli
76 is the upregulation of IE-genes, including the viral transcription factor ORF50/K-Rta, which
77 instigates the lytic infection state. ORF50/K-Rta is known to robustly activate various lytic
78 gene promoters, including E-genes (21, 22). The subsequent expression of E-genes leads to

79 replication of the viral DNA genome, as certain E-genes encode viral DNA polymerase factor
80 proteins. This process then paves the way for the transcription of L-genes, encoding various
81 viral structural proteins (*e.g.*, capsid, tegument, and envelope proteins), and ensuring the
82 efficient production of progeny virus particles (6, 23).

83 A unique regulatory system for the expression of L-genes has been observed in gamma-
84 and beta-herpesviruses, but not in alpha-herpesviruses. Most viruses employ the host
85 transcription machinery, including the pre-initiation complex (PIC) consisting of TATA-
86 binding protein (TBP) bound to specific DNA sequences, and general transcription factors
87 (GTFs), which utilize the host PIC machinery for the expression of IE- and E-genes.
88 Conversely, these 2 herpesvirus subfamilies rely on a viral PIC (vPIC) for the transcription of
89 some L-genes (24-26).

90 In KSHV, 6 viral proteins (ORF18, ORF24, ORF30, ORF31, ORF34, and ORF66) have
91 been identified as components of vPIC (27-33). KSHV ORF24 is thought to be a functional
92 analog of TBP, since ORF24 directly binds to a TATA-box-like DNA sequence known as the
93 TATT motif, which is present at the transcription start site (TSS) of some L-genes (25). ORF24
94 recruits the RNA polymerase II (RNAPII) complex to the L-gene TSS and initiates mRNA
95 transcription (28, 34). In contrast, KSHV ORF34 interacts directly with ORF24 and serves as
96 a binding platform for several PIC components, namely ORF18, ORF31, and ORF66 (27-33).
97 ORF30 seems to directly bind only to ORF18, as association with the other vPIC components
98 has not been detected (28, 33, 35). Each component of this protein complex is indispensable
99 for the expression of the L-gene, which is essential for infectious virus production (27-33).
100 However, the precise interaction mechanism among each vPIC component and the stepwise
101 process of assembly into the complete vPIC remain to be elucidated. In addition to recruiting
102 RNAPII to the L-gene TSS, other functions of vPIC are poorly understood.

103 Our previous study explored the role of KSHV ORF34 in viral replication, revealing it

104 as a binding platform for vPIC components (27). We demonstrated that the central region of
105 ORF34 was critical for binding to ORF18, ORF31, and ORF66. We also found that the C-
106 terminal region of ORF34 was necessary for interaction with ORF24 and virus production.
107 These results indicate that ORF34 assembles several vPIC components (ORF18, ORF31, and
108 ORF66) via its middle region, and its C-terminus harnesses them to ORF24 to form a vPIC at
109 the L-gene TSS. However, detailed information regarding the molecular structure of ORF34
110 and its contribution to its function remains unknown.

111 To elucidate how the microstructure and/or domain structure of ORF34 influences its
112 physiological functions, a deep-learning-based structural model of ORF34 was initially
113 generated. This model predicted a tetrahedral arrangement of the 4 conserved cysteines (C170,
114 C175, C256, and C259) in ORF34 that are potentially instrumental in the incorporation of metal
115 cations. Subsequent experimental evaluation of this predicted model demonstrated that these
116 conserved cysteines were instrumental in vPIC assembly, late gene transcription, and viral
117 production.
118

119 **Results**

120 **Predicted structure model of KSHV ORF34 utilizing deep-learning algorithm and**
121 **identification of conserved amino-acid residues between ORF34 and beta- and gamma-**
122 **herpes viral homologs**

123 Based on our previous study (27), we attempted to further investigate the functional
124 regions of ORF34, a key component of the viral pre-initiation complex (vPIC). These findings
125 are expected to provide more precise insights into the functions and mechanisms of KSHV
126 ORF34 and vPIC. In the realm of life sciences, including virology, deep-learning algorithms
127 have been widely used as powerful tools for predicting protein structure models, and we applied
128 this approach in our early work on a partial vPIC protein-protein interaction model (35). In this
129 study, we derived a structure for KSHV ORF34 using Alphafold2 (AF2), an algorithm capable
130 of predicting protein structure based on amino acid sequences (36). The resulting predicted
131 structure was visualized using an illustration model color-labeled with pLDDT, representing
132 the prediction confidence score (Fig. 1a and 1b). Furthermore, using AF2 and the related
133 module, we visualized the predicted aligned error (PAE) plot, which provides insights into
134 domain prediction by illustrating the predicted distances between alpha-carbon positions for
135 each amino acid pair (Fig. 1c). The green pixels in the PAE plot represent the predicted distance
136 errors between the alpha carbons of the amino acid pairs. Consequently, the presence of green
137 signal areas indicates clustering of amino acid residues that likely form distinct domains. Based
138 on our KSHV ORF34 predicted model, the PAE plot suggested the existence of a small domain
139 in the N-terminal region (approximately 1-50 a.a.) and a larger domain structure in the C-
140 terminal region (approximately 110-327 a.a.) (Fig. 1c). Additionally, this plot indicated that a
141 disordered region (approximately 50-110 a.a.) connects the N-terminal- and C-terminal
142 domains of ORF34 (Fig. 1c). Disordered regions in proteins are typically characterized by the
143 absence of stable tertiary structures, and thus provide flexible linkages between domains with

144 defined structures. In the illustration model with pLDDT (Fig1a and 1b), the predicted
145 disordered region corresponded to the string and helix (labeled orange–yellow), indicating low
146 prediction reliability.

147 As previously described, the vPIC machinery and its viral components are broadly
148 conserved across beta- and gamma-herpesvirus families (24, 26). It has been hypothesized that
149 critical domains or structures in each functioning protein, such as vPIC components, are
150 conserved among viral homologs. In general, these conserved domains and structures often
151 contain conserved amino acid residues. To ascertain the conserved amino acid residues, we
152 performed sequence alignments of the KSHV ORF34 amino acid residues with other herpes
153 virus homologs (Fig. 2a), which highlighted these conserved residues against a gray
154 background. We discovered 7 amino-acid residues at the N-terminus and 21 at the C-terminus
155 of KSHV ORF34 that were conserved among beta- and gamma-herpesviruses. Thus, to analyze
156 the roles of these conserved residues in ORF34 function, we prepared 18 expression plasmids
157 with single or double alanine substitutions at the conserved amino acid residues to generate
158 ORF34 alanine-scanning mutants, after excluding the conserved prolines to avoid disrupting
159 the local and whole protein backbone (Fig. 2a). Based on the relationships between conserved
160 residues and the predicted structure of ORF34, we generated a histogram displaying the
161 pLDDT score against the amino acid residues of ORF34 with dotting on the conserved residues
162 targeted for the alanine mutations described above (Fig. 2b). The histogram confirmed that the
163 local structural features surrounding these conserved residues were predicted with high
164 confidence, meaning that all conserved residues were localized in a highly structured domain,
165 the N-term region, and the C-term region, as suggested (Fig. 1c). We prepared 18 expression
166 plasmids with single or double alanine substitutions at the conserved amino acid residues to
167 generate ORF34 alanine-scanning mutants, after excluding the conserved prolines to avoid
168 disrupting the local and whole protein backbone (Fig. 2).

169

170 **Physical interactions between ORF34 alanine-scanning mutants and vPIC components**

171 KSHV ORF34 has been reported to directly interact with the majority of vPIC
172 components (ORF18, ORF24, ORF31, and ORF66), with the exception of ORF30 (27, 28).
173 Based on these findings, KSHV ORF34 is thought to be a hub protein that forms vPIC. To
174 analyze the contribution of ORF34 conserved residues to the interaction with other vPIC
175 components, binding between ORF34 alanine-scanning mutants and the other components was
176 assessed through pull-down experiments (Figs. 3 and 4).

177 The N-terminal region (1-400 a.a.) of ORF24 (ORF24 binding domain; ORF24 BD)
178 binds to ORF34, with R328 on ORF24 being essential for ORF34 binding (28). To facilitate
179 ORF24 detection, we prepared expression plasmids of ORF24 BD (6xMyc-tagged ORF24 BD
180 [1-400 a.a.]). 293T cells were co-transfected with 2xS-tagged ORF34 alanine-scanning
181 mutants and 6xMyc-ORF24 BD, 3xFLAG-ORF66, 3xFLAG-ORF18, and 3xFLAG-ORF31,
182 as indicated in each figure, and cell extracts were then subjected to pull-down experiments.
183 Initially, we profiled the interaction ability of the ORF34 mutants with ORF24 BD and ORF66.
184 Our ORF34 mutants exhibited various features associated with another vPIC component.
185 Notably, ORF34 C170A, C175A, C256A, and C259A remarkably decreased or lost their
186 binding abilities to ORF24 and ORF66 (Fig. 3b-c and 3e-f). In addition, G165A,
187 L188A/L189A, Y194A, and Q264A/N265A also lost their interactions with ORF66 (Fig. 3d-
188 f). Conversely, no defects in the interaction between ORF18 and ORF31 were observed in any
189 of the ORF34 alanine-scanning mutants (Fig. 4). Our previous study using ORF34 deletion
190 mutants showed that the 100-150 a.a. region of ORF34 is responsible for binding to ORF18
191 and ORF31 (27). However, the ORF34 alanine-scanning mutants in the present study did not
192 include any alanine-substituted residues in that region. Therefore, the binding data for the
193 ORF34 alanine-scanning mutants in the present study yielded concordant results.

194

195 **Characterization of ORF34 conserved residues concerning KSHV production**

196 Because transcriptional initiation through the vPIC is essential for KSHV production,
197 we considered progeny virus production to be the most appropriate method for evaluating the
198 functional importance of ORF34 conserved residues in vPIC. Therefore, a complementation
199 assay was conducted using ORF34-deficient virus-producing cells stably expressing ORF34
200 alanine-scanning mutants.

201 First, we established iSLK cell lines harboring KSHV ΔORF34-BAC (iSLK-Δ34) and
202 iSLK cell lines harboring KSHV ΔORF34 revertant-BAC (iSLK-Δ34Rev). BACmids were
203 constructed as described in our previous study (27). 3xFLAG-tagged ORF34 WT were
204 transfected with the iSLK-Δ34 cells. The control plasmid was transfected into iSLK-Δ34 and
205 iSLK-Δ34Rev cells. To generate stable cell lines, the transfected cells were subjected to drug
206 selection, and complemented exogenous ORF34 in iSLK-Δ34 cells was confirmed (Fig. 5a).
207 Using these cell lines, we evaluated the recovery ability of exogenous ORF34 in iSLK-Δ34
208 cells (Fig. 5b) and cultured them in conditioned medium containing sodium butyrate (NaB; an
209 HDAC inhibitor that accelerates gene expression) and doxycycline (Dox, an activator of the
210 Tet-on system) for 3 days. Using this system in an iSLK cell, Dox induced ORF50/k-RTA,
211 thereby triggering the lytic phase). The encapsidated KSHV genome was purified from the
212 cultured supernatant and quantified by quantitative polymerase chain reaction (qPCR).

213 The results showed that ORF34 deficiency causes a notable decrease in virus
214 production, and exogenous ORF34 in deficient cells complements most virus production.
215 These results underscore the need for ORF34 in KSHV viral production.

216 The same strategy was employed to evaluate 18 conserved amino acid mutants of
217 ORF34. Each FLAG-tagged ORF34 mutant expression plasmid was transfected into iSLK-Δ34
218 cells and selected for the generation of stable cell lines, as indicated, and protein expression

219 was confirmed (lower panels in Fig. 5c-e). KSHV production in these cell lines was then
220 compared with that in iSLK-Δ34/ORF34 WT cells (upper graphs in Fig. 5c-e). The results
221 showed that complementation with ORF34 G165A, S168A, and G182A rescued virus
222 production in iSLK-Δ34 cells, indicating that these substituted residues do not contribute to the
223 ORF34 role in virus release. In contrast, ORF34 E41A/T42A-, F47A-, D154A-, C170A-,
224 C175A-, L188A/L189A-, C256A-, C259A-, Q264A/N265A-, and Y310A-expressing cell lines
225 did not show recovered virus production, indicating that these mutated residues contribute to
226 the ORF34 wild-type role in virus release. Exogenous ORF34 V50A, W160A, Y194A, Y215A,
227 and R234A partially complemented the loss of ORF34 in the iSLK-Δ34 cells.
228
229 **Role of ORF34 conserved residues in viral gene transcription and protein expression**
230 The main function of vPIC in the KSHV life cycle is to initiate L-gene expression. To
231 determine whether the virus production recovery abilities of ORF34 WT and mutants were due
232 to KSHV L-gene expression, we analyzed the expression of the representative genes in each
233 step (*i.e.,* K4 as IE, ORF6 as E, and K8.1 as L-gene) based on the mRNA (Fig. 6a-c) and protein
234 expression (Fig. 6d-f). The stable cell lines, iSLK-Δ34 cells complemented with ORF34 WT
235 or alanine-scanning mutants, were stimulated with NaB and Dox for 3 days. Total RNA was
236 extracted from each cell line and subjected to reverse transcription quantitative PCR (RT-
237 qPCR).
238 The results showed that the transcription of K8.1 in iSLK-Δ34 cells expressing ORF34
239 E41A/T42A, F47A, D154A, C170A, C175A, L188A/L189A, Y194A, C256A, C259A,
240 Q264A/N265A, and Y310A was markedly reduced compared with that in iSLK-Δ34/WT cells,
241 but differed little from that in iSLK-Δ34/control cells. In contrast, the transcription of K8.1,
242 complemented by G165A, S168A, G182A, and Y215A (Fig. 6a-c). The transcription levels of
243 K4 and ORF6 were almost equal in all iSLK-Δ34 cell lines expressing ORF34 WT or its

244 mutants. In parallel with RNA sampling, we prepared protein samples from each
245 complemented iSLK-Δ34 cell line. The protein expression of the representative E gene K-bZIP
246 in each cell line showed no marked differences among cell lines (Fig. 6d-f; upper middle
247 panels). In contrast, we observed notable differences in K8.1 protein expression among the cell
248 lines. The K8.1 protein expression was rescued in ORF34 G165A-, S168A-, and Y215A-
249 expressing iSLK-Δ34 cell lines and was partially complemented in ORF34 R234A- and
250 G182A-expressing cells. The protein expression of K8.1 was unable not be rescued in other
251 mutants (Fig. 6d-f; upper panels). These differences in K8.1 protein expression among cell
252 lines were consistent with the data on K8.1 mRNA obtained by qPCR.
253
254 **Contribution of ORF34 conserved residues for recruitment to K8.1 transcription start**
255 **site**
256 vPIC formation at the TSS of L-genes is essential for the expression of the L-genes. To
257 assess the influence of substitution of conserved residues for ORF34 recruitment to K8.1-TSS,
258 we evaluated the association of ORF34 WT and mutants with K8.1-TSS in the lytic state of the
259 KSHV genome. The stable cell lines, iSLK-Δ34 cells complemented with ORF34 WT or
260 alanine-scanning mutants, were stimulated with NaB and Dox for 3 days. The lytic-induced
261 cell lines were subjected to ChIP with Contorol IgG or anti-FLAG antibody and then subjected
262 to qPCR (ChIP-qPCR) (Fig. 7a-c).
263 The results demonstrated that the association of ORF34 with K8.1-TSS in iSLK-Δ34
264 cells expressing ORF34 F47A and S168A was clearly higher than that in iSLK-Δ34/WT cells.
265 The complement abilities of E41A/T42A, G165A, G182A, and Y215A were almost the same
266 as those of the ORF34 WT. The remaining cell lines complemented with the mutants V50A,
267 D154A, W160A, C170A, C175A, L188A/L189A, Y194A, R234A, C256A, C259A,
268 Q264A/N265A, and Y310A, showed a decline in the enrichment of K8.1-TSS in comparison

269 to iSLK-Δ34/ WT cells, but did not reach the basal level (*e.g.*, iSLK-Δ34/control cells) (Fig.
270 7a-c).
271
272 **Profiling of ORF34 alanine-scanning mutants on vPIC-related parameters**
273 The data obtained in this study (Fig. 3, 5-7) were summarized and visualized using a
274 heatmap with a dendrogram of hierarchical clustering (Fig. 8a). The extracted parameters were
275 as follows: i) binding to ORF66 (Fig. 3d-f), ii) binding to ORF24BD (Fig. 3a-e), iii) K8.1
276 mRNA expression (Fig. 6a-e), iv) K8.1A/B protein expression (Fig. 6d-f), v) KSHV production
277 (Fig. 5c-e), and vi) ORF34 recruitment to K8.1-TSS (Fig. 7a-c). Binding to ORF18 and ORF31
278 (Fig. 4) was excluded because no differences between ORF34 WT and its mutant were
279 observed. ORF34 mutants were roughly classified into 4 groups according to the visualized
280 dendrogram (Fig. 8a). In parallel, we also calculated the relative solvent-accessible surface area
281 (relative-SASA), the indicator of amino-acid residues exposed on the protein surface, based on
282 the ORF34 prediction model (Fig. 8b). The classified residues are highlighted in the illustration
283 (Fig. 9a) or illustration-surface model of the predicted ORF34 (Fig. 9b).
284 Group 1: Mutants complemented virus production in iSLK-Δ34 cells. Thus, these
285 substituted amino acid residues are not essential for vPIC function.
286 Group 2: The mutants maintained their binding to ORF24 (but not to ORF66) and failed
287 to complement virus production. These mutated sites may be related to vPIC function via
288 ORF66 binding. It is possible that these mutated sites are related to the vPIC function via
289 ORF66 binding.
290 Group 3: The mutants failed to complement virus production and showed decreased
291 binding to both ORF24 and ORF66. Conserved residues in the mutants were inferred to be
292 essential for vPIC function via complex formation.
293 Group 4: While the mutants did not rescue virus production, their binding ability to

294 ORF24 and ORF66 was unaltered. Thus, these mutation sites are important for the vPIC
295 machinery. The mechanism underlying the contribution of these residues to vPIC function
296 might not involve a direct interaction with ORF24 and ORF66. However, the precise details of
297 this process remain unknown.

298 The S168A and F47A mutants were out of the range of the other mutants in the
299 dendrogram. The ORF34 S168A mutant showed over-complementation in virus production
300 and K8.1-TSS recruitment, approximately 13 and 2.2 times more than ORF34 WT, respectively.
301 Almost equal to ORF34 WT, ORF34 S168A showed binding abilities to ORF24 and ORF66.
302 Therefore, further studies on S168 are necessary to clarify the mechanisms of vPIC regulation.
303 The ORF F47A mutant also demonstrated over-complementation in K8.1-TSS recruitment,
304 namely it was more than 6 times higher than that of ORF34WT. However, the F47A mutant
305 failed to complement L-gene transcription, protein expression, or virus production. The ORF34
306 F47 residue, present in the predicted N-term domain, may have roles in vPIC-mediated
307 transcription or vPIC assembly, other than the direct association with other vPIC components.

308 G165A, G182A, and Y215A, classified as Group 1, reduced the interaction with ORF66
309 and maintained or mildly reduced viral production. Therefore, these sites likely contribute to
310 the association between the2 viral proteins, ORF34 and ORF66. However, considering the
311 small influence on virus production, L-gene expression, and L gene TSS assembly in each
312 KSHV-producing cell line, other factors brought about by viral infection, including vPIC
313 components, might help restore the association between ORF34 G165A/G182A/Y215A and
314 ORF66 in virus-producing cells.

315 The mutants classified into Group 2, D154A, W160A, L188A/L199A, Y194A,
316 Q264A/Q265A, and Y310A, showed little recovery of virus production, an almost deficient
317 vPIC function, a mild decrease in association with ORF24, and a decrease in ORF66 (Fig. 3-
318 8a). Prediction models suggest that these mutated sites are included in the inner side of the C-

319 terminal domain, and only N265 was exposed to the protein surface (Fig. 8b and Fig. 10). Thus,
320 these mutated residues are responsible for supporting the backbone of the C-terminal domain
321 structure.

322 All ORF34 mutants, which maintained a minimum binding ability to ORF24, were
323 enriched in the L-gene TSS to some extent (Fig. 7a-c and 8a), although their expression was
324 not fully correlated with the degree of association with ORF24BD (Fig. 3a-c and 8a). However,
325 the mutants in groups 2, 3, and 4 failed to recover viral production. This suggests that the
326 mutated residues of groups 2 and 3 contribute to the vPIC function for virus production via an
327 association with ORF66, and mutated residues of group 4 operate in vPIC via other
328 mechanisms.

329 At a minimum, our data (Fig. 3, 5-7) and grouping of ORF34 mutants by hierarchical
330 clustering (Fig. 8a) demonstrated that ORF34 C170A, C175A, C256A, and C259A, which
331 were categorized into Group 3, lost most of their interactions with ORF24 and ORF66 and the
332 virus production recovery ability. This suggests that these conserved cysteines, which were
333 predicted to have little exposure to the protein surface (Fig. 8b and 9a-b), are crucial for ORF34
334 function in KSHV replication.

335

336 **Four conserved cysteine residues in the predicted ORF34 structure**

337 Among the conserved amino acids, 4 cysteines (C170, C175, C256, and C259) were
338 predicted to be present in the C-terminal domain (Fig. 1c and 2b), including the inner side of
339 the protein (Fig. 8b and 9). The precise position and side chain were visualized and enlarged
340 (Fig. 10a). On reframing these residues in an amino acid sequence (Fig. 2a), C170-R171-A172-
341 D173-C174-C175 and C256-L257-L258-C259 form the consensus motif sequences C-X_4-C
342 and C-X_2-C, respectively. These 2 consensus sequences (C-X_n-C) are known to form ion-
343 capturing domains such as the zinc finger domain. Furthermore, in the prediction model, we

344 found that the pairs of consensus C-X_n-C motifs exhibited nearly symmetrical positioning
345 within ORF34 (Fig. 10a), suggesting the potential for metal cation capture.

346 To simulate the ion-binding affinity resulting from the conserved cysteine residues in
347 our ORF34 structural model, we estimated potential binding ions by employing a Metal Ion-
348 Binding site prediction and modeling server (37). Docking simulation predicted the binding
349 residues of ORF34 with 16 metals and 18 ions. We identified metal ions that were captured by
350 residues within at least one of the consensus sequence cysteines (C170-C175 and/or C256-
351 C259) and had predicting scores > 3.0 (Fig. 10b). Of the 18 ions tested, 7 (Zn^{2+}, Fe^{2+}, Fe^{3+},
352 Cd^{2+}, Hg^{2+}, Cu^{+}, and Pb^{2+}) were predicted to be captured by at least 1 of the C-Xn-C ORF34
353 motifs. Notably, 3 metal ions (Zn^{2+}, Fe^{2+}, and Fe^{3+}) were expected to be captured by all 4
354 conserved cysteine residues (Fig. 10b), with the binding score indicating a dominant interaction
355 between ORF34 and Zn^{2+} ions.

356 Next, we attempted to confirm that metal ion capture is crucial for ORF34 to function
357 as a hub protein in vPIC. The *in vitro* binding ability of ORF34 to ORF24 or ORF66 was
358 analyzed in the presence of the chelating agent, TPEN, which has a higher affinity for heavy
359 metal ions, including Zn, Fe, and Mn, than for Ca and Mg. The stability constant, a chemical
360 indicator of chelating ability, of TPEN was the highest for Zn among the 5 metal ions. Our
361 results showed that TPEN interferes with ORF34 association not only with ORF24 BD (Fig.
362 10c) but also with ORF66 (Fig. 10d) in a concentration-dependent manner. These results
363 suggested that capturing the heavy metal cation via conserved cysteines contained in the C-X_n-
364 C consensus motif is important for the binding of ORF34 to other vPIC components (ORF24
365 and ORF66).

366

367

368 **Discussion**

369 In this study, we constructed alanine-substituted mutants of KSHV ORF34 with
370 conserved amino acid residues and assessed their roles in viral replication and vPIC formation.
371 After obtaining diverse information from our results, it is noteworthy that the 4 conserved
372 cysteines (C170, C175, C256, and C259) in KSHV ORF34 are essential for the vPIC machinery.
373 The mutants KSHV ORF34 C170A, C175A, C256A, and C259A were deficient in their
374 association with ORF24 and ORF66 (Fig. 3 and 8a). Furthermore, these mutants failed to
375 complement virus production (Fig. 5 and 8a) and K8.1 gene transcription and protein
376 expression (Fig. 6 and 8a) but also reduced recruitment to K8.1-TSS (Fig.7 and 8a). The
377 conserved cysteines of ORF34 may have some physical or virological significance in protein
378 structure and function. One of the findings supporting this speculation is that the 4 cysteines
379 comprised 2 pairs of C-X_n-C consensus sequences (C170 and C175, and C256 and C259) (Fig.
380 2a). Second, the deep-learning-structure model predicted that the conserved cysteines are
381 present on the inner side of ORF34 (Fig. 8b, 9a-b, and 10a) and are placed in a roughly
382 tetrahedral formation (Fig. 9 and 10a). Using the AlphaFold2 prediction model as our query,
383 another prediction method (Metal Ion-Binding site prediction and modeling server; MIB2)
384 provided data supporting the high probability of ion holding by ORF34 conserved cysteines
385 (Fig. 9b). This prediction demonstrated that the top candidate metal cation captured by the
386 double pair of conserved cysteines of ORF34 was zinc (Fig. 9b).

387 Further supporting the speculation concerning the physical or virological significance
388 of the conserved cysteines, the binding ability of ORF34 to ORF24 and ORF66 was decreased
389 in the presence of TPEN, a heavy metal cation chelator (Fig. 9c and 9d). Because TPEN has a
390 higher affinity for zinc cations than iron, it can exclude captured zinc more efficiently than iron
391 and other metal cations. An article regarding the mathematical prediction of the ion-binding
392 site of metalloproteins revealed that AlphaFold2 is a useful and extensive tool for protein

393 annotation of zinc ion binding (38). This report endorses our analysis strategy for annotating
394 the 4 conserved cysteines of ORF34 as binding sites for metal cations. Despite the lack of direct
395 evidence, our prediction models and data from chelator treatment suggest that zinc was
396 captured by ORF34 conserved cysteines. Concrete evidence concerning protein structure,
397 including the ion positions as determined by X-ray crystallography, nuclear magnetic
398 resonance (NMR), or Cryogenic Electron Microscopy (Cryo-EM), is indispensable for
399 confirming these findings.

400 For host proteins composing cellular PIC, the functional analog of vPIC, capturing the
401 ions is also important. Cellular PIC consist of TBP, GTFs, and multiple subunits of the RNAPII
402 complex. Holding zinc via C-X_n-C motifs has been reported in several factors of cellular PIC,
403 including TFIIEα (39), TFIIB (40), TFIIS (41), and RPB9 (RNAPII subunit 9) (42). In TFIIEα,
404 the loss of capturing ions induces a structural disturbance that negatively influences its
405 binding ability to other factors and its transcription capability (39, 43). Zinc binding to TFIIB
406 affects the structural rigidity and protein surface charge around the zinc-binding domain (44).
407 Furthermore, the C-X_n-C motif is indispensable for other vPIC components. We and Didychuck
408 *et al.* demonstrated the importance of the C-X_n-C sequence of ORF66 in viral replication via
409 vPIC formation (30, 31). In summary, the present findings and previous reports of host cellular
410 PIC factors strongly support the notion that ion capture via the C-X_n-C motif on the KSHV
411 ORF34 protein is crucial for maintaining the structural character and binding ability of ORF34
412 to other vPIC components, resulting in virus production via L-gene expression using vPIC
413 machinery.

414 Our functional profiling of the ORF34 conserved residues provided other valuable
415 findings. KSHV ORF34 conserved residues E41/T42 and V50, which were classified into
416 Group 4 (Fig. 8a), and F47, which were not classified (Fig. 8a), were present in the ORF34 N-
417 terminus (fig.2a). E41/T42 and V50 were essential residues for viral replication via L-gene

418 expression but did not affect associations with other vPIC components (Fig. 3-8a). F47 had
419 almost the same tendency as other N-terminal residues, but F47A showed a significant increase
420 in the K8.1 promoter. A simple speculation concerning the roles of these residues is that they
421 are associated with unknown host factors, which contribute to the modulation of vPIC-
422 mediated transcription. The predicted algorithm AlphaFold2 suggested that ORF34 has an N-
423 terminal domain and a C-terminal domain separated by the disordered region (Fig. 1a-b and
424 2b). E41/T42, F47, and V50 exist in the N-terminal domain (Fig. 2b and 9a-b). The other
425 conserved amino acid residues, including those responsible for binding to other vPIC
426 components, ORF24 and ORF66, exist in the C-terminal domain (Fig. 2b, 8a, 9a-b). Other
427 prediction algorithms for the disordered region, PrDOS (45) and DISOPRED3 (46), also
428 suggested the presence of disordered regions of KSHV ORF34 at 64-70/89-108 a.a. and 92-
429 107 a.a., respectively. Homology search results using the PDB database in the running process
430 of AlphaFold2 demonstrated a similarity between the N-terminal domain and some regulatory
431 factors of the RNAPII complex.

432 Another hypothesis concerning the conserved N-terminal residues is based on EBV
433 studies. It was reported that the phosphorylated T42 residue of BGLF3 (KSHV ORF34
434 homolog) is essential for vPIC function and that phospho-T42 of BGLF3 is important for sub-
435 complex formation among BFRF2 (KSHV ORF66 homolog) and BVLF1 (KSHV ORF18
436 homolog) (47). These reports demonstrated that 2 molecular interactions, BGLF3 binding to
437 BFRF2 or BVLF1, were not affected by the phosphorylation state of T42, but 3 molecular
438 interactions, the presence of BGLF3, BFRF2, and BVLF1, were positively dependent on
439 phospho-T42 (47). Our alanine mutant, ORF34 E41A/T42A, harbors a mutation in analogous
440 residues of EBV BGLF3 T42. Our observations of the ORF34 E41A/T42A mutant, including
441 interaction analysis, gene expression, and virus production, were well matched with a previous
442 EBV study (47). Unfortunately, whether the subcomplex (*i.e.,* a subset of a larger functional

443 protein complex) is present in KSHV has not yet been confirmed. Phospho-T42 in KSHV
444 ORF34 may contribute to subcomplex formation, and the residues surrounding T42 (E41, F47,
445 and V50) may also work in coordination. However, further research on this topic is required.
446 Another characteristic finding was the conservation of serine and tyrosine residues in
447 the KSHV ORF34. First, the ORF34 serine residue mutant S168A showed a better ability for
448 virus production than ORF34 WT (Fig.5 and 8a). Previous studies on vPIC factors among
449 herpesviruses have identified multiple serine/threonine residues in EBV BDLF4 (KSHV
450 ORF31 homolog) (48). If phosphorylation occurs on KSHV ORF34, S168 phosphorylation is
451 related to the dysregulation of vPIC. Second, the ORF34 tyrosine residue mutants, Y194A and
452 Y310A, lost their ability to bind to ORF66, L-gene expression, translocate to the L-gene TSS,
453 and virus release, but did not lose their ability to bind to ORF18, ORF24, and ORF31 (Fig. 3-
454 8a). Thus, phosphorylation of Y194 and Y310 may be related to the positive regulation of
455 ORF66 binding. However, the prediction model did not indicate the full exposure of the side
456 chains of these residues, S168, Y194, and Y310, to the surface of ORF34 (Fig. 8b and 9a-b).
457 To determine whether phosphorylation of ORF34 occurs, real experimental data are necessary.
458 Phosphorylation and other post-translational modifications might also contribute to vPIC
459 regulation.
460 Our results demonstrate the importance of the 4 conserved cysteine residues in the
461 KSHV ORF34 protein for functional vPIC, following KSHV ORF66 (30, 31). Our evidence
462 and structure prediction suggest that these 4 cysteines would contribute to cation capturing,
463 which might be essential for maintaining the conformation of ORF34 as a scaffold for vPIC
464 formation. In addition, we can speculate about the functional possibilities of the character
465 profiling of the ORF34 mutants and the predicted structure. The N-terminal domain of ORF34
466 may be associated with unknown host factors and may bundle multiple vPIC components. On
467 the other hand, according to our prediction model, our experimental strategy using conserved

residue mutations would not fully cover the associated protein surface. Thus, adequate proof has not yet been obtained, and further efforts are necessary to answer questions concerning this complex.

Material and Methods

Protein structure prediction and ion binding prediction and modeling

The KSHV ORF34 protein structure model was predicted using AlphaFold 2.2.0 software program (https://github.com/deepmind/alphafold) in the local environment (36). The following databases were used for AlphaFold2: Uniclust30 (version 2018_08), MGnify (version 2018_12), pdb70 (downloaded on Feb 15th, 2022), PDB/mmCIF (downloaded on Feb 18th, 2022), and pdb_seqres (downloaded on Feb 18th, 2022). Notably, several versions or frequently updated versions of these databases have been utilized. The predicted model was visualized using the molecular visualization open-source software program PyMOL (ver. 2.5.0). In addition, the pLDDT score coloring of the predicted model was visualized with the python module "PSICO" (https://github.com/speleo3/pymol-psico). Visualization of the PAE plot was completed using the Python module "plddt2csv" (https://github.com/CYP152N1/plddt2csv). To predict disordered protein regions of KSHV ORF34, PrDOS (https://prdos.hgc.jp/cgi-bin/top.cgi) and DISOPRED3 (http://bioinf.cs.ucl.ac.uk/psipred) have also been used (45, 46). The relative per-residue solvent-accessible surface area was calculated using the `get_sasa_relative` syntax in open-source PyMOL 2.1, with default settings of dot density of 2 and solvent radius of 1.4.

The metal ion-binding (MIB) site prediction and modeling server (http://bioinfo.cmu.edu.tw/MIB/) was used to predict the binding residues of 18 different metal ions (Ca^{2+}, Cu^{+}, Cu^{2+}, Fe^{2+}, Fe^{3+}, Mg^{2+}, Mn^{2+}, Zn^{2+}, Cd^{2+}, Ni^{2+}, Hg^{2+}, Co^{2+}, Au^{+}, Ba^{2+}, Pb^{2+}, Pt^{2+}, Sm^{3+}, and Sr^{2+}) in the protein (37, 49). The query of the protein structure was compared to metal-ion binding templates, which allowed MIB residues within at least 3.5 Å of the ion to be predicted, along with a binding score and template. Template with the highest binding score (> 3.0) was documented if the same binding residue was present multiple times for a single metal ion.

499

500 *Cell culture and reagents*

501 293T cells (RCB2202; RIKEN BioResource Center, Tsukuba, Japan) were cultured in
502 the growth medium. DMEM was supplemented with 10% fetal calf serum and a penicillin-
503 streptomycin solution (Nacalai Tesque Inc., Kyoto, Japan). The transfection reagent for 293T
504 cells, PEI-MAX MW40000 (Polysciences, Inc., Warrington, PA, U.S.A.), was dissolved at a
505 concentration of 1 mg/mL in distilled water and filtered.

506

507 *Plasmids*

508 The pCI-neo-2xS-ORF34 WT, pCI-neo-3xFLAG-ORF66, pCI-neo-3xFLAG-ORF18,
509 and pCI-neo-3xFLAG-ORF31 expression plasmids have been described previously (27).
510 Alanine scanning mutants of ORF34 coding fragments were obtained by PCR or overlap-
511 extension PCR from the KSHV ORF34 expression plasmid using the primer sets indicated in
512 Table 1. To construct pCI-neo-6xMyc-ORF24-BD (1-400), partial ORF24 coding fragments
513 (1-400 a.a.) containing the ORF34 binding region (28) were also obtained by PCR from the
514 KSHV ORF24 expression plasmid. These fragments were cloned into expression plasmids
515 based on a pCI-neo mammalian expression vector (Promega, Madison, WI, U.S.A.), *e.g.* pCI-
516 neo-2xS, pCI-neo-6xMyc, or pCI-blast-3xFLAG.

517

518 *Establishment of doxycycline-inducible recombinant KSHV-expressing cells and stably ORF34*
519 *WT- and mutant-expressing cells*

520 For maintenance, iSLK cells were cultured in growth medium of DMEM/fetal calf serum 10%
521 containing 1 μg/mL puromycin (Fujifilm-Wako Chemicals, Osaka, Japan) and 0.25 mg/mL of
522 G418 (Fujifilm-Wako Chemicals). The KSHV BAC16 mutant (ΔORF34-BAC16) and its
523 revertant (ΔORF34Rev-BAC16), as previously described (27), were transfected into iSLK

524 cells using Screenfect A plus (Fujifilm-Wako Chemicals) according to the manufacturer's
525 instructions. Transfected cells were selected using 1000 μg/mL of hygromycin B (Fujifilm
526 Wako Chemicals) to establish doxycycline-inducible recombinant KSHV-producing cell lines
527 (iSLK-Δ34Rev and iSLK-Δ34).

528 To establish stable ORF34-expressing cells for complementation, pCI-blast-3xFLAG-
529 ORF34 and empty vector pCI-blast-3xFLAG were transfected into iSLK-Δ34Rev and iSLK-
530 Δ34 cells, and transfected cells were selected and maintained in 10 μg/mL and 7.5 μg/mL of
531 Blasticidin S (Fujifilm-Wako Chemicals), respectively. Thus, stable cell lines iSLK-
532 Δ34Rev/pCI-blast-3xFLAG, iSLK-Δ34/pCI-blast-3xFLAG, iSLK-Δ34/pCI-blast-3xFLAG-
533 ORF34WT, and iSLK-Δ34/pCI-blast-3xFLAG-ORF34 mutants were established.

534

535 *Measurement of KSHV production*

536 To quantify virus production, KSHV virions in the culture supernatant were quantified as
537 described previously (27, 30, 50, 51) with minor modifications. Briefly, iSLK-harboring KSHV
538 BAC cells were treated with 0.75 mM NaB and 4 μg/mL doxycycline for 72 h to induce lytic
539 replication and production of recombinant KSHV, and culture supernatants were harvested.
540 The culture supernatants (150 μL) were treated with DNase I (NEB, Ipswich, MA, U.S.A.) to
541 obtain enveloped and encapsidated viral genomes. Viral DNA was purified and extracted from
542 100 μL of DNase I-treated culture supernatant using a QIAamp DNA Blood Mini Kit
543 (QIAGEN GmbH, Hilden, Germany). To quantify viral DNA copies, SYBR Green real-time
544 PCR was performed using THUNDERBIRD Next SYBR qPCR Mix (TOYOBO, Osaka,
545 Japan) with KSHV-encoded ORF11 specific primers (27, 30).

546

547 *Quantification of viral gene expression*

548 To assess the roles of ORF34 WT and its mutants in viral gene expression, RT-qPCR was

549 performed as previously described (30). iSLK-Δ34 cells complemented with ORF34 WT or its
550 mutants were stimulated and cultured, as described in the previous section. Total RNA was
551 extracted from the treated cell lines using Sepasol-RNA II super (Nacalai Tesque, Inc.). Total
552 RNA was digested with DNase using the ReverTra Ace qPCR RT Master Mix with gDNA
553 Remover (TOYOBO) to exclude host and viral genomic DNA (gDNA), which interfered with
554 mRNA quantification as a background. cDNA was synthesized using the same kit and subjected
555 to SYBR green real-time PCR using the THUNDERBIRD Next SYBR qPCR Mix (TOYOBO)
556 and the primer sets listed in Table 1, based on Fakhari and Dittmer (52) and the selected unique
557 CDS referenced by Bruce *et al.* (53). Relative KSHV mRNA expression was determined using
558 the GAPDH expression and ΔΔCt methods.
559
560 *Western blotting, pull-down assays, and antibodies*
561 To detect viral proteins, iSLK-Δ34 cells complemented with ORF34 WT or mutants were
562 stimulated and cultured, as described in the previous section. The treated cells were washed
563 with PBS, directly lysed with W.B. sample buffer, and boiled. The W.B. samples were then
564 subjected to western blotting, as described previously (30).
565 Pull-down assays between vPIC components and ORF34 were performed as previously
566 described (27, 30, 35). Briefly, 293T cells were transfected with the indicated plasmids using
567 PEI-MAX (54) and cultured for 2 days. Transfected cells were lysed using lysis buffer (20 mM
568 HEPES (pH 7.9), 0.18 M NaCl, 0.1% (v/v) NP-40, 10% (v/v) Glycerol, 0.1 mM EDTA) with
569 protease inhibitors and briefly sonicated to destroy the cell nucleus. Whole-cell extract, which
570 is the supernatant obtained from the lysate centrifuged to discard cell debris, was subjected to
571 affinity purification using S-protein-agarose (Merck Millipore, Burlington, MA, U.S.A.) for 1–
572 2 h and washed 4 times. Purified precipitates, including bait and prey proteins (2xS-tagged
573 ORF34 WT/mutants and their counterparts) binding to S-protein-agarose, and whole-cell

574 extracts were subjected to western blotting.

575 Treatment of the vPIC interaction with the zinc chelator TPEN (*N*,*N*,*N′*,*N′*-tetrakis (2-
576 pyridylmethyl) ethylenediamine; TCI, Tokyo, Japan) was also performed as described
577 previously (30). Briefly, 293T cell lysates transfected with 2xS-ORF34 or control vector were
578 subjected to S-protein-agarose purification in the presence of each dose of TPEN or vehicle
579 (ethanol). The beads associated with bait protein ORF34 WT or control were mixed with the
580 cell lysate of prey proteins (6xMyc-ORF24BD or 3xFLAG-ORF66) and overexpressed in
581 293T cells in the presence of each dose of TPEN or vehicle. Beads were washed 4 times and
582 subjected to western blot analysis.

583 Anti-Myc (9E10; Santa-Cruz, CA, U.S.A.), anti-S-tag pAb (MBL, Nagoya, Japan),
584 anti-FLAG (DDDDK-tag) (FLA-1; MBL), Anti-HHV8 K-bZIP (F33P1; Santa-Cruz), Anti-
585 HHV8 K8.1A/B (4A4; Santa Cruz), and anti-β-Tubulin (10G10; Fujifilm-Wako Chemicals)
586 were used as the primary antibodies. HRP-linked anti-mouse IgG antibody (Jackson
587 ImmunoResearch, Inc., West Grove, PA, U.S.A.) and HRP-linked anti-rabbit IgG antibody
588 (Jackson ImmunoResearch, Inc.) were used as the secondary antibodies. Antibody-bound
589 proteins were visualized using ECL Western Blotting Detection Reagents (ATTO, Tokyo,
590 Japan) on an X-ray film (FUJIFILM Corp., Tokyo, Japan).

591 The pull-down efficiency score indicated that the band intensity of the prey protein
592 (ORF24BD, ORF66) obtained from the mean region of interest using the ImageJ software
593 program (Version; 2.0.0-rc-43/1.52n) was normalized to that of the bait protein (ORF34
594 WT/mutants).

595

596 *ChIP-qPCR*

597 To survey the recruitment of ORF34 to the TSS of the L gene, iSLK-Δ34 cells complemented
598 with ORF34 WT or mutants were subjected to ChIP with several minor modifications of

599 previous methods (30). Complemented iSLK-Δ34 cells with ORF34 WT or mutants were
600 stimulated and cultured as described above virus production section. A total of 1.2 × 10^6 cells
601 of each iSLK-Δ34-complemented cell line were seeded onto 10 cm dishes and stimulated with
602 10 mL of growth medium containing 0.75mM NaB and 4μG/mL Dox for 72 h. The cells were
603 washed once and supplemented with 10 mL of pre-warmed 2% FCS medium. 11xFixation
604 buffer (1 mL) containing methanol-free formaldehyde (#11850-14; Nacalai Tesque) (11.1%
605 formaldehyde, 50 mM HEPES (pH8.0), 100 mM NaCl, 1 mM EDTA, 0.5 mM EGTA) was
606 directly added to culture dishes and incubated for 10 min at room temperature, then sequentially
607 quenched by 1mL of 1.5 M glycine. The fixed cells were washed with ice-cold PBS 3 times
608 and Farnham Buffer (5mM PIPES (pH8.0), 85mM KCl, 0.5% (v/v) NP-40) with protease
609 inhibitor cocktail (#25955-11; Nacalai Tesque) and scraped from dishes. The cells were
610 homogenized in a 25-gauge syringe, and the pellet was washed with Farnham buffer. The cell
611 nuclear pellets were suspended into 440 μL SDS-lysis buffer (50 mM Tris (pH8.0), 10 mM
612 EDTA, 1% (w/v) SDS), sonicated by Bio-Raptor (High, 30 s; ON, 30 s; OFF, ×6 cycles) and
613 centrifuged to remove debris. Cell nuclear extracts were diluted 10 times by ChIP Dilution
614 Buffer (50 mM Tris (pH8.0), 167mM NaCl, 1.1% (v/v) Triton X-100, 0.11% (w/v) sodium
615 deoxycholate). The diluted extracts were pre-cleared with 30 μL of Protein G Sepharose
616 (Cytiva, Tokyo, Japan). The supernatants (1.2 mL) were subjected to immunoprecipitation with
617 30 μG of protein G magnetic beads (Dynabeads Protein G, Thermo Scientific) overnight. The
618 magnetic beads were pre-conjugated with 2 mg/sample of normal mouse IgG (Santa Cruz
619 Biotechnology) or anti-FLAG monoclonal antibody (M2; Sigma) for approximately 6-8 hours
620 in 0.5% BSA/PBS solution. The IP-subjected magnetic beads were washed with RIPA buffer
621 (50 mM Tris (pH8.0), 150 mM NaCl, 1mM EDTA, 1% (v/v) Triton X-100, 0.1% (w/v) SDS,
622 0.1% (w/v) sodium deoxycholate) twice, RIPA high-salt buffer (50 mM Tris (pH8.0), 500 mM
623 NaCl, 1mM EDTA, 1% (v/v) Triton X-100, 0.1% (w/v) SDS, 0.1% (w/v) sodium deoxycholate),

624 LiCl buffer (10 mM Tris (pH8.0), 250 mM LiCl, 1mM EDTA, 0.5% (v/v) NP-40, 0.5% (w/v)
625 sodium deoxycholate), TE buffer (10 mM Tris (pH8.0), 1mM EDTA), and TE buffer containing
626 0.5% RIPA buffer. Finally, 120 μL of ChIP direct elution buffer (10 mM Tris (pH8.0), 300 mM
627 NaCl, 5mM EDTA, 0.5% (w/v) SDS) was added to the magnetic beads and incubated overnight
628 at 65°C for de-crosslinking. As a 1% input sample, 12 μL of the diluted extracts was diluted 10
629 times with ChIP direct elution buffer and subjected to de-crosslinking and after-treatments in
630 parallel with the magnetic bead samples. The samples were digested with RNase A and
631 Proteinase K at 37°C and 55°C, respectively. DNA was extracted from 110 μL of the digested
632 supernatant using a Gel/PCR purification kit (Nihon Genetics) with minor modifications,
633 column binding DNA was washed twice, and eluted with 75 μL of the kit elution buffer. The
634 extracted DNA solutions were subjected to qPCR using primers for the K8.1-TSS (30).
635
636 *Statistical analyses and data visualization*
637 The standard deviation was determined by analyzing the data obtained from 3 independent
638 samples, and is indicated as error bars. Welch's *t*-test was used to determine differences
639 between the indicated groups. p-values are shown in the figure. For the functional profile
640 analysis of ORF34 WT and its mutants, a heatmap with a dendrogram that highlights
641 hierarchical clustering was visualized using R (Ver 4.0.3) and R Studio with R package
642 "Superheat" (https://rlbarter.github.io/superheat/)(55).
643
644 *Data Availability*
645 The data that support the findings of this study are available from the corresponding author,
646 T.W., upon reasonable request.
647

Acknowledgments

BAC16, a KSHV BAC clone, was a kind gift from Dr. Jae U Jung (Lerner Research Institute of Cleveland Clinic, U.S.A.). We also thank Dr. Gregory A. Smith (Northwestern University, U.S.A.) for providing the *E. coli* strain GS1783.

This work was partially supported by JSPS Grant-in-Aid for Scientific Research (C) (JP21K08509; T.W. and JP19K07669; S.O.), Takeda Science Foundation (T.W.), The Association for Research on Lactic Acid Bacteria (S.O.), the University of the Ryukyus Research Project Promotion Grant for Young Researchers (20SP04102; T.W.), the Research Start-up and the CAS Faculty Mellon Fund from American University (T.I.), and the National Institutes of Health through a grant from the National Institute of Allergy and Infectious Diseases (7R15AI172610; T.I.).

In this work, we would also like to thank Ms. Kazumi Tamaki, who is a member of the University of the Ryukyus integrated technology center, for her valuable technical support and documental management related to our laboratory work.

664 **References**

665 1. Pellett PE, Davison, A.J., Eberle, R., Ehlers, B., Hayward, G.S., Lacoste, V., Minson,
666 A.C., Nicholas, J., Roizman, B., Studdert, M.J. and Wang, F. 2011. Order *Herpesvirales*.
667 *In* King A, Lefkowitz E., Adams, M.J., Carstens, E.B. (ed), Virus Taxonomy: Ninth
668 Report of the International Committee on Taxonomy of Viruses. Elsevier.
669 2. Pellett PE, Davison, A.J., Eberle, R., Ehlers, B., Hayward, G.S., Lacoste, V., Minson,
670 A.C., Nicholas, J., Roizman, B., Studdert, M.J., Wang, F. 2011. Family *Herpesviridae*,
671 p 81-92. *In* King A, Lefkowitz E., Adams, M.J., Carstens, E.B. (ed), Virus Taxonomy:
672 Ninth Report of the International Committee on Taxonomy of Viruses. Elsevier.
673 3. Krug LT, Pellet PE. 2022. The family Herpesviridae: A Brief introduction, p 212-234.
674 *In* Knipe DM, Howley PM, Damania BA, Cohen JI (ed), Fields Virology, 7th Edition,
675 vol 2. Lippincott Williams & Wilkins.
676 4. Wen KW, Wang L, Menke JR, Damania B. 2021. Cancers associated with human
677 gammaherpesviruses. FEBS J doi:10.1111/febs.16206.
678 5. Gewurz BE, Longnecker RM, Cohen JI. 2022. Epstein-Barr Virus, p 324-388. *In* Knipe
679 DM, Howley PM, Damania BA, Cohen JI (ed), Fields Virology, 7th Edition, vol 2.
680 Lippincott Williams & Wilkins.
681 6. Damania BA, Cesarman E. 2022. Kaposi's Sarcoma Herpesvirus, p 513-572. *In* Knipe
682 DM, Howley PM, Damania BA, Cohen JI (ed), Fields Virology, 7th Edition, vol 2.
683 Lippincott Williams & Wilkins.
684 7. Cesarman E, Damania B, Krown SE, Martin J, Bower M, Whitby D. 2019. Kaposi
685 sarcoma. Nat Rev Dis Primers 5:9.
686 8. Cesarman E, Chadburn A, Rubinstein PG. 2022. KSHV/HHV8-mediated hematologic
687 diseases. Blood 139:1013-1025.
688 9. Wen KW, Damania B. 2010. Kaposi sarcoma-associated herpesvirus (KSHV):
689 molecular biology and oncogenesis. Cancer Lett 289:140-50.
690 10. Arias C, Weisburd B, Stern-Ginossar N, Mercier A, Madrid AS, Bellare P, Holdorf M,
691 Weissman JS, Ganem D. 2014. KSHV 2.0: a comprehensive annotation of the Kaposi's
692 sarcoma-associated herpesvirus genome using next-generation sequencing reveals
693 novel genomic and functional features. PLoS Pathog 10:e1003847.
694 11. Song MJ, Li X, Brown HJ, Sun R. 2002. Characterization of interactions between RTA
695 and the promoter of polyadenylated nuclear RNA in Kaposi's sarcoma-associated
696 herpesvirus/human herpesvirus 8. J Virol 76:5000-13.
697 12. Chang PJ, Shedd D, Gradoville L, Cho MS, Chen LW, Chang J, Miller G. 2002. Open
698 reading frame 50 protein of Kaposi's sarcoma-associated herpesvirus directly activates
699 the viral PAN and K12 genes by binding to related response elements. J Virol 76:3168-
700 78.
701 13. Cai X, Lu S, Zhang Z, Gonzalez CM, Damania B, Cullen BR. 2005. Kaposi's sarcoma-

associated herpesvirus expresses an array of viral microRNAs in latently infected cells. Proceedings of the National Academy of Sciences 102:5570-5575.

14. Tagawa T, Gao S, Koparde VN, Gonzalez M, Spouge JL, Serquiña AP, Lurain K, Ramaswami R, Uldrick TS, Yarchoan R, Ziegelbauer JM. 2018. Discovery of Kaposi's sarcoma herpesvirus-encoded circular RNAs and a human antiviral circular RNA. Proc Natl Acad Sci U S A 115:12805-12810.
15. Cohen JI. 2020. Herpesvirus latency. J Clin Invest 130:3361-3369.
16. Gunther T, Grundhoff A. 2010. The epigenetic landscape of latent Kaposi sarcoma-associated herpesvirus genomes. PLoS Pathog 6:e1000935.
17. Toth Z, Maglinte DT, Lee SH, Lee HR, Wong LY, Brulois KF, Lee S, Buckley JD, Laird PW, Marquez VE, Jung JU. 2010. Epigenetic analysis of KSHV latent and lytic genomes. PLoS Pathog 6:e1001013.
18. Toth Z, Brulois K, Jung JU. 2013. The chromatin landscape of Kaposi's sarcoma-associated herpesvirus. Viruses 5:1346-73.
19. Jenner RG, Alba MM, Boshoff C, Kellam P. 2001. Kaposi's sarcoma-associated herpesvirus latent and lytic gene expression as revealed by DNA arrays. J Virol 75:891-902.
20. Guito J, Lukac DM. 2012. KSHV Rta Promoter Specification and Viral Reactivation. Front Microbiol 3:30.
21. Miller G, El-Guindy A, Countryman J, Ye J, Gradoville L. 2007. Lytic Cycle Switches of Oncogenic Human Gammaherpesviruses, p 81-109 doi:10.1016/s0065-230x(06)97004-3.
22. Sun R, Lin SF, Gradoville L, Yuan Y, Zhu F, Miller G. 1998. A viral gene that activates lytic cycle expression of Kaposi's sarcoma-associated herpesvirus. Proc Natl Acad Sci U S A 95:10866-71.
23. Hancock MH, Skalsky RL. 2018. Roles of Non-coding RNAs During Herpesvirus Infection. Curr Top Microbiol Immunol 419:243-280.
24. Dremel SE, Didychuk AL. 2023. Better late than never: A unique strategy for late gene transcription in the beta- and gammaherpesviruses. Semin Cell Dev Biol 146:57-69.
25. Nandakumar D, Glaunsinger B. 2019. An integrative approach identifies direct targets of the late viral transcription complex and an expanded promoter recognition motif in Kaposi's sarcoma-associated herpesvirus. PLoS Pathog 15:e1007774.
26. Gruffat H, Marchione R, Manet E. 2016. Herpesvirus Late Gene Expression: A Viral-Specific Pre-initiation Complex Is Key. Front Microbiol 7.
27. Nishimura M, Watanabe T, Yagi S, Yamanaka T, Fujimuro M. 2017. Kaposi's sarcoma-associated herpesvirus ORF34 is essential for late gene expression and virus production. Sci Rep 7:329.
28. Davis ZH, Hesser C, Park J, Glaunsinger BA. 2015. Interaction Between ORF24 and

ORF34 in the Kaposi's Sarcoma-Associated Herpesvirus Late Gene Transcription Factor Complex is Essential For Viral Late Gene Expression. J Virol doi:10.1128/jvi.02157-15.

29. Brulois K, Wong LY, Lee HR, Sivadas P, Ensser A, Feng P, Gao SJ, Toth Z, Jung JU. 2015. Association of Kaposi's Sarcoma-Associated Herpesvirus ORF31 with ORF34 and ORF24 Is Critical for Late Gene Expression. J Virol 89:6148-54.

30. Watanabe T, Nishimura M, Izumi T, Kuriyama K, Iwaisako Y, Hosokawa K, Takaori-Kondo A, Fujimuro M. 2020. Kaposi's Sarcoma-Associated Herpesvirus ORF66 Is Essential for Late Gene Expression and Virus Production via Interaction with ORF34. J Virol 94.

31. Didychuk AL, Castaneda AF, Kushnir LO, Huang CJ, Glaunsinger BA. 2020. Conserved CxnC Motifs in Kaposi's Sarcoma-Associated Herpesvirus ORF66 Are Required for Viral Late Gene Expression and Are Essential for Its Interaction with ORF34. J Virol 94.

32. Gong D, Wu NC, Xie Y, Feng J, Tong L, Brulois KF, Luan H, Du Y, Jung JU, Wang CY, Kang MK, Park NH, Sun R, Wu TT. 2014. Kaposi's sarcoma-associated herpesvirus ORF18 and ORF30 are essential for late gene expression during lytic replication. J Virol 88:11369-82.

33. Castañeda AF, Glaunsinger BA. 2019. The Interaction between ORF18 and ORF30 Is Required for Late Gene Expression in Kaposi's Sarcoma-Associated Herpesvirus. J Virol 93:e01488-18.

34. Davis Zoe H, Verschueren E, Jang Gwendolyn M, Kleffman K, Johnson Jeffrey R, Park J, Von Dollen J, Maher MC, Johnson T, Newton W, Jäger S, Shales M, Horner J, Hernandez Ryan D, Krogan Nevan J, Glaunsinger Britt A. 2015. Global Mapping of Herpesvirus-Host Protein Complexes Reveals a Transcription Strategy for Late Genes. Mol Cell 57:349-360.

35. Maeda Y, Watanabe T, Izumi T, Kuriyama K, Ohno S, Fujimuro M. 2022. Biomolecular Fluorescence Complementation Profiling and Artificial Intelligence Structure Prediction of the Kaposi’s Sarcoma-Associated Herpesvirus ORF18 and ORF30 Interaction. Int J Mol Sci 23:9647.

36. Jumper J, Evans R, Pritzel A, Green T, Figurnov M, Ronneberger O, Tunyasuvunakool K, Bates R, Zidek A, Potapenko A, Bridgland A, Meyer C, Kohl SAA, Ballard AJ, Cowie A, Romera-Paredes B, Nikolov S, Jain R, Adler J, Back T, Petersen S, Reiman D, Clancy E, Zielinski M, Steinegger M, Pacholska M, Berghammer T, Bodenstein S, Silver D, Vinyals O, Senior AW, Kavukcuoglu K, Kohli P, Hassabis D. 2021. Highly accurate protein structure prediction with AlphaFold. Nature 596:583-589.

37. Lu C-H, Chen C-C, Yu C-S, Liu Y-Y, Liu J-J, Wei S-T, Lin Y-F. 2022. MIB2: metal ion-binding site prediction and modeling server. Bioinformatics 38:4428-4429.

38. Wehrspan ZJ, McDonnell RT, Elcock AH. 2022. Identification of Iron-Sulfur (Fe-S) Cluster and Zinc (Zn) Binding Sites Within Proteomes Predicted by DeepMind's AlphaFold2 Program Dramatically Expands the Metalloproteome. J Mol Biol 434:167377.
39. Okuda M, Tanaka A, Arai Y, Satoh M, Okamura H, Nagadoi A, Hanaoka F, Ohkuma Y, Nishimura Y. 2004. A novel zinc finger structure in the large subunit of human general transcription factor TFIIE. J Biol Chem 279:51395-403.
40. Chen HT, Legault P, Glushka J, Omichinski JG, Scott RA. 2000. Structure of a (Cys3His) zinc ribbon, a ubiquitous motif in archaeal and eucaryal transcription. Protein Sci 9:1743-52.
41. Qian X, Jeon C, Yoon H, Agarwal K, Weiss MA. 1993. Structure of a new nucleic-acid-binding motif in eukaryotic transcriptional elongation factor TFIIS. Nature 365:277-279.
42. Wang B, Jones DN, Kaine BP, Weiss MA. 1998. High-resolution structure of an archaeal zinc ribbon defines a general architectural motif in eukaryotic RNA polymerases. Structure 6:555-69.
43. Okuda M, Tanaka A, Hanaoka F, Ohkuma Y, Nishimura Y. 2005. Structural insights into the asymmetric effects of zinc-ligand cysteine mutations in the novel zinc ribbon domain of human TFIIEalpha for transcription. J Biochem 138:443-9.
44. Ghosh M, Elsby LM, Mal TK, Gooding JM, Roberts SG, Ikura M. 2004. Probing Zn2+-binding effects on the zinc-ribbon domain of human general transcription factor TFIIB. Biochem J 378:317-24.
45. Ishida T, Kinoshita K. 2007. PrDOS: prediction of disordered protein regions from amino acid sequence. Nucleic Acids Res 35:W460-4.
46. Jones DT, Cozzetto D. 2015. DISOPRED3: precise disordered region predictions with annotated protein-binding activity. Bioinformatics 31:857-63.
47. Li J, Walsh A, Lam TT, Delecluse HJ, El-Guindy A. 2019. A single phosphoacceptor residue in BGLF3 is essential for transcription of Epstein-Barr virus late genes. PLoS Pathog 15:e1007980.
48. Sato Y, Watanabe T, Suzuki C, Abe Y, Masud H, Inagaki T, Yoshida M, Suzuki T, Goshima F, Adachi J, Tomonaga T, Murata T, Kimura H. 2019. S-Like-Phase Cyclin-Dependent Kinases Stabilize the Epstein-Barr Virus BDLF4 Protein To Temporally Control Late Gene Transcription. J Virol 93.
49. Lu CH, Lin YF, Lin JJ, Yu CS. 2012. Prediction of metal ion-binding sites in proteins using the fragment transformation method. PLoS One 7:e39252.
50. Wakao K, Watanabe T, Takadama T, Ui S, Shigemi Z, Kagawa H, Higashi C, Ohga R, Taira T, Fujimuro M. 2014. Sangivamycin induces apoptosis by suppressing Erk signaling in primary effusion lymphoma cells. Biochem Biophys Res Commun

816 444:135-40.
817 51. Watanabe T, Nakamura S, Ono T, Ui S, Yagi S, Kagawa H, Watanabe H, Ohe T,
818 Mashino T, Fujimuro M. 2014. Pyrrolidinium fullerene induces apoptosis by activation
819 of procaspase-9 via suppression of Akt in primary effusion lymphoma. Biochem
820 Biophys Res Commun 451:93-100.
821 52. Fakhari FD, Dittmer DP. 2002. Charting Latency Transcripts in Kaposi's Sarcoma-
822 Associated Herpesvirus by Whole-Genome Real-Time Quantitative PCR. J Virol
823 76:6213-6223.
824 53. Bruce AG, Barcy S, DiMaio T, Gan E, Garrigues HJ, Lagunoff M, Rose TM. 2017.
825 Quantitative Analysis of the KSHV Transcriptome Following Primary Infection of
826 Blood and Lymphatic Endothelial Cells. Pathogens (Basel, Switzerland) 6:11.
827 54. Katoh Y, Nozaki S, Hartanto D, Miyano R, Nakayama K. 2015. Architectures of
828 multisubunit complexes revealed by a visible immunoprecipitation assay using
829 fluorescent fusion proteins. J Cell Sci 128:2351-62.
830 55. Barter RL, Yu B. 2018. Superheat: An R package for creating beautiful and extendable
831 heatmaps for visualizing complex data. J Comput Graph Stat 27:910-922.
832

833

834 **Figure legends**

835 **Fig. 1. The ORF34 structure model predicted by Alphafold2 and conserved cysteines on**
836 **ORF34.** The predicted ORF34 structure was visualized, and the predicted domain structure
837 was analyzed. (a) The ORF34 structure was predicted using the deep-learning algorithm
838 Alphafold2 (AF2). The illustration depicts the protein labeled with colors according to the
839 pLDDT score of each amino-acid residue. (b) Rotation of the predicted ORF34 structure model
840 that was depicted in (a). (c) Prediction alignment error (PAE) plot of the predicted ORF34
841 structure. Each white to green pixel indicates a predicted distance of, 30 to 0 Å respectively,
842 between amino-acid residues.

843

844 **Fig. 2. Conserved amino-acid residues of ORF34 homolog and alanine-scanning mutants.**
845 Amino acid sequence alignment of KSHV ORF34. Herpesvirus homolog amino acid sequences
846 were translated from nucleotide sequences found in the NCBI database (KSHV ORF34 (JSC-
847 1-BAC16; Accession number GQ994935), MHV68 ORF34 (strain WUMS; NC_001826),
848 EBV BGLF3 (strain B95-8; V01555), CMV UL95 (strain Towne; FJ616285), HHV6B U67
849 (strain japan-a1; KY239023)). Raw data regarding alignment were obtained using Clustal
850 Omega (EMBL-EBI; https://www.ebi.ac.uk/Tools/msa/clustalo/). Completely conserved
851 amino acids between homologs are indicated by a gray background. Based on the alignment
852 information, 1-2 conserved amino acids residues, except for proline and alanine, were
853 substituted with alanine for ORF34 alanine-scanning mutants, as depicted. (b) The histogram
854 of the pLDDT score demonstrated by AF2 on each amino-acid residue on ORF34 (1-327 a.a.),
855 the conserved amino-acid residues are indicated with white circles.

856

857 **Fig. 3. Physical interactions between ORF34 alanine-scanning mutants and vPIC**
858 **components, ORF24 and ORF66.** 293T cells were co-transfected with expression plasmids

859 of the 2xS-ORF34 alanine-scanning mutant and 6xMyc-ORF24BD (a-c) or 3xFLAG-ORF66
860 (d-f). ORF24BD corresponds to the KSHV ORF24 N-terminal domain (1-400 a.a.) reported as
861 having a domain interaction with ORF34 (28). Transfected cells were lysed, and cell lysates
862 were subjected to pull-down assays using S-protein-agarose that captured the 2xS-ORF34
863 mutants. Obtained precipitates including 2xS-ORF34 mutants were probed with indicated
864 antibodies to detect interactions. Whole cell extracts (WCEs) were also probed as the input
865 controls of prey proteins for each sample. The pull-down efficiency score of each interaction
866 was indicated below the pull-down panel of prey proteins (6xMyc-ORF24BD or 3xFLAG-
867 ORF66). The pull-down efficiency score of the sample co-transfected with ORF34 WT and
868 ORF24BD/ORF66 was defined as 1.0. N.D. (not detected) indicates that a positive signal of
869 the prey proteins was not detected.
870
871 **Fig. 4. Physical interaction between ORF34 alanine-scanning mutants and vPIC**
872 **components, ORF18 and ORF31.** 293T cells were co-transfected with expression plasmids
873 of 2xS-ORF34 alanine-scanning mutant and 3xFLAG-ORF18 (a-c) or 3xFLAG-ORF31 (d-f).
874 Transfected cells were lysed and cell lysates were subjected to pull-down assays using S-
875 protein-agarose that captured the 2xS-ORF34 mutants. Obtained precipitates including 2xS-
876 ORF34 mutants were probed with the indicated antibodies to detect interactions. Whole cell
877 extracts (WCEs) were also probed as the input controls of prey proteins for each sample.
878
879 **Fig. 5. Complement abilities of ORF34 alanine-scanning mutants on viral production.**
880 Establishment of 3xFLAG-tagged ORF34-expressing iSLK-Δ34 stable cell lines and
881 confirmation of the recovery by ORF34 WT in ΔORF34-virus production. (a) The Western blot
882 showed exogenous 3xFLAG-tagged ORF34 WT expression in iSLK-Δ34 cells. (b) A
883 complementation assay was performed to rescue virus production. (c-e) 3xFLAG-tagged

884 ORF34 alanine-scanning mutant-expressing iSLK-Δ34 stable cell lines were investigated for
885 their virus production recoveries, with results shown in the upper graph panels. The lower blot
886 panels indicate the exogenous ORF34 WT/mutant expression under normal culture conditions.
887 In the upper graph panels, the virus production of iSLK-Δ34/ORF34 WT cells was defined as
888 100%. Each stable iSLK-KSHV BAC-harboring cell line was activated by NaB (0.75 mM) and
889 Dox (4 μG/mL) and cultured for 3 days, and the culture supernatant containing encapsidated
890 KSHV genome was harvested and quantified. Three independent samples were evaluated by
891 real-time PCR and indicated as dots in each column. The error bars indicate standard deviations.
892
893 **Fig. 6. Complement abilities of ORF34 alanine-scanning mutants for viral gene**
894 **transcription and protein expression.** The mRNA and protein expression in lytic-induced
895 iSLK-Δ34 cells complemented with ORF34 WT/alanine-scanning mutants. The cells were
896 cultured for 3 days in conditioned medium containing NaB and Dox to induce a lytic state. (a-
897 c) Total RNA was extracted from cells and subjected to RT-qPCR. The mRNA expression of
898 viral genes, which is representative of each step (K4 as IE gene, ORF6 as E gene, K8.1 as L-
899 gene), was normalized by GAPDH expression. The mRNA expression of iSLK-
900 ΔORF34/control cells with NaB and Dox treatment was defined as 1.0. Four independent
901 samples were evaluated and indicated as dots in each column. The error bars indicate standard
902 deviations. (d-e) Total protein samples were prepared from each lytic-induced cell and
903 subjected to Western blotting. The protein expression of the L-gene was analyzed by K8.1A/B
904 blotting and the E gene by K-bZIP, respectively. The protein expression score, the band
905 intensity, of iSLK-Δ34/ORF34 WT was defined as 1.0. N.D. (not detected), indicating that a
906 positive signal of viral proteins was not detected.
907
908 **Fig. 7. Recruitment of ORF34 alanine-scanning mutants to late gene transcription start-**

909 **site.** The binding quantity of the KSHV late gene TSS to ORF34 WT/alanine-scanning mutants
910 was evaluated by ChIP. The iSLK-Δ34 cells complemented with ORF34 WT/alanine-scanning
911 mutants were cultured for 3 days in conditioned medium containing NaB and Dox to induce a
912 lytic state. (a-c) A KSHV DNA fragment precipitated by control mouse IgG or anti-FLAG
913 monoclonal antibody was subjected to RT-qPCR and normalized by input DNA subjected to
914 ChIP. Each fold enrichment of iSLK-ΔORF34/control cells by control IgG or anti-FLAG
915 antibodies was defined as 1.0. Three independent samples were evaluated and indicated as dots
916 in each column. The error bars indicate standard deviation.
917
918 **Fig. 8. Summary of the effects of ORF34 alanine-scanning mutants on the vPIC function.**
919 (a) The results (Fig. 5, 5-7) were summarized and visualized on the heatmap with a dendrogram
920 highlighting the hierarchical clustering. Each score of ORF34 WT or iSLK-Δ34/WT was
921 defined as 1.0. The scores are indicated on each panel with the color gradient (dark blue [0.0]
922 - green [1.0] - yellow [>3.0]) as indicated by the lower bar. N.D. (not detected) in each
923 experiment is indicated by the gray panel. Groups were classified according to the visualized
924 dendrogram. (b) Based on the ORF34 structure model (Fig.1a), the prediction score of protein
925 surface exposure, relative solvent accessible surface area (relative-SASA), were listed for each
926 mutated site. The relative-SASA score colored with orange [>0.1] indicates that the amino-acid
927 residue has a high possibility of being exposed on the protein surface.
928
929 **Fig. 9. Overview of the predicted ORF34 structure and mutated residues.** Rotated ORF34
930 structures with caption based on the predicted structure (Fig 1a and 1b) (a) In the illustration
931 model, all the mutated amino-acid residues are highlighted with colors according to the
932 grouping (Fig. 8a), and captioned. (b) In the surface-illustration model based on (a), only the
933 mutated amino-acid residues expected to be exposed on protein surface (Fig. 8b) are captioned.

934

935 **Fig. 10. The prediction of metal cation binding to ORF34 and its influence on the binding**
936 **ability of ORF34.** (a) The table organizes the binding residues, templates, and binding scores
937 of 18 different metal ions predicted by the Metal Ion-Binding site prediction and modeling
938 server, MIB2. When multiple copies of identical binding residues were present for a single
939 metal ion, the template with the highest binding score was noted. If any new binding residues
940 were present amongst previously recorded ones, the template was still recorded. Prediction
941 binding scores higher than 3.0 are listed. Conserved cysteine residues (C170, C175, C256,
942 C256) were highlighted with magenta. (b) Predicted model of ORF34 structure binding to ions.
943 The illustration model of ORF34 was visualized according to Fig. 7a (right panel), and the
944 binding zinc ion (Zn^{2+}) is shown as a gray sphere. Heavy metal cation chelation influences the
945 ORF34 binding abilities to ORF24BD (c) and ORF66 (d). Pull-down assays using S-tagged
946 ORF34 binding beads as bait in the presence of cell extracts overexpressed prey proteins
947 (6xMyc-ORF24BD or 3xFLAG-ORF66) and the heavy metal chelator TPEN. The pull-down
948 efficiency score is indicated below the pull-down panel of the prey protein. The score of the
949 sample co-incubated with 2xS-ORF34 WT binding beads as bait and 6xMyc-ORF24BD or
950 3xFLAG-ORF66 as prey was defined as 1.0.

951

Table 1: Primers for Construction of expression plasmids and RT-qPCR

Primer name	Primer sequences (5' -> 3')
[Cloning expression plasmid]	*a
S-EcoRI-kshvORF34	acatgaattcATGTTTGCTTTGAGCTCGC
As-kshvORF34-SalI	ctaagtcgacTTAGAGTTGGTTGAGTCCATTCTCC
S_MluI-ORF24BD(1-400)	catacgcgtATGGCAGCGCTCGAGGGC
As_ORF24BD(1-400)-XbaI	taatctagaTTAGCCCAGAGTCCGCGCGTCCGTG
- ORF34 Alanin-scanning mutants	*b
S_ORF34_Asc1_E41AT42A	tgataGCAGCTcccctgaacag
As_ORF34_Asc1_E41AT42A	ggggAGCTGCtatcaacttaaattgtc
S_ORF34_Asc2_F47A	aacagcGCCctcttggtttcc
As_ORF34_Asc2_F47A	caagagGGCgctgttcaggg
S_ORF34_Asc3_V50A	ctcttgGCAtccaacgtgatgc
As_ORF34_Asc3_V50A	ttggaTGCcaagaggaagctg
S_ORF34_Asc4_D154A	ctgacGCCccccttccgttg
As_ORF34_Asc4_D154A	gggGGCgtcaggaagaagac
S_ORF34_Asc5_W160A	gttgctaGCGctgctgttcaac
As_ORF34_Asc5_W160A	agcagCGCtagcaacggaag
S_ORF34_Asc6_G165A	tgttcaacGCTcccgcctc
As_ORF34_Asc6_G165A	gcgggAGCgttgaacagcag
S_ORF34_Asc7_S168A	acccgccGCGttttgtcg
As_ORF34_Asc7_S168A	acaaaaCGCggcgggtcc
S_ORF34_Asc8_C170A	ctttGCTcgggccgactgttg
As_ORF34_Asc8_C170A	gcccgAGCaaaagaggcgg
S_ORF34_Asc9_C175A	gactgtGCCctgtacaagcagc
As_ORF34_Asc9_C175A	gtacagGGCacagtcggccc
S_ORF34_Asc10_G182A	gcagcactgcGCAtacccg
As_ORF34_Asc10_G182A	cgggtaTGCgcagtgctgc
S_ORF34_Asc11_L188AL189A	gtgGCAGCTccaggtcacatg
As_ORF34_Asc11_L188AL189A	gAGCTGCcaccgggccc
S_ORF34_Asc12_Y194A	catgGCCgctcccaaacgg
As_ORF34_Asc12_Y194A	ggagcGGCcatgtgacctgg
S_ORF34_Asc13_Y215A	gtttctaGCCggagatttttccggg
As_ORF34_Asc13_Y215A	ctccGGCtagaaacttggtgtacttc
S_ORF34_Asc14_R234A	gctacttctGCCatacaaagggtagtgag
As_ORF34_Asc14_R234A	ctttgtatGGCagaagtagcgaatggc
S_ORF34_Asc15_C256A	acaccGCCctcttgTGTcacatatatc
As_ORF34_Asc15_C256A	agagGGCggtgtgggaaatg
S_ORF34_Asc16_C259A	cctgcctcttgGCTcacatatatcag
As_ORF34_Asc16_C259A	tgtgAGCcaagaggcaggtgtg
S_ORF34_Asc17_Q264AN265A	tcagGCAGCTagcataattgcggg
As_ORF34_Asc17_Q264AN265A	atgctAGCTGCctgatatatgtgacac
S_ORF34_Asc18_Y310A	catcgGCTgacataccggcgatc
As_ORF34_Asc18_Y310A	atgtcAGCcgatgggatgattagatag
[RT-qPCR]	
qPCR_K4-F	TTGTCCGGTCTATGCCAGG
qPCR_K4-R	CTGCCTTGCTTTGTTTGCAA
qPCR_ORF6-F	CTGCCATAGGAGGGATGTTTG
qPCR_ORF6-R	CCATGAGCATTGCTCTGGCT
qPCR_K8.1-F	ACAGATTCGCACAGAAATCCCT
qPCR_K8.1-R	CGAACGATACGTGGGACAATTG
qPCR_GAPDH-F	TCGCTCTCTGCTCCTCCTGTTC
qPCR_GAPDH-R	CGCCCAATACGACCAAATCC

**a*: Underlined lowercase indicates a restriction enzyme site, while uppercase indicates a protein-coding sequence

**b*: Underlined uppercase indicates a mutagenesis site.

Fig.1

(a)

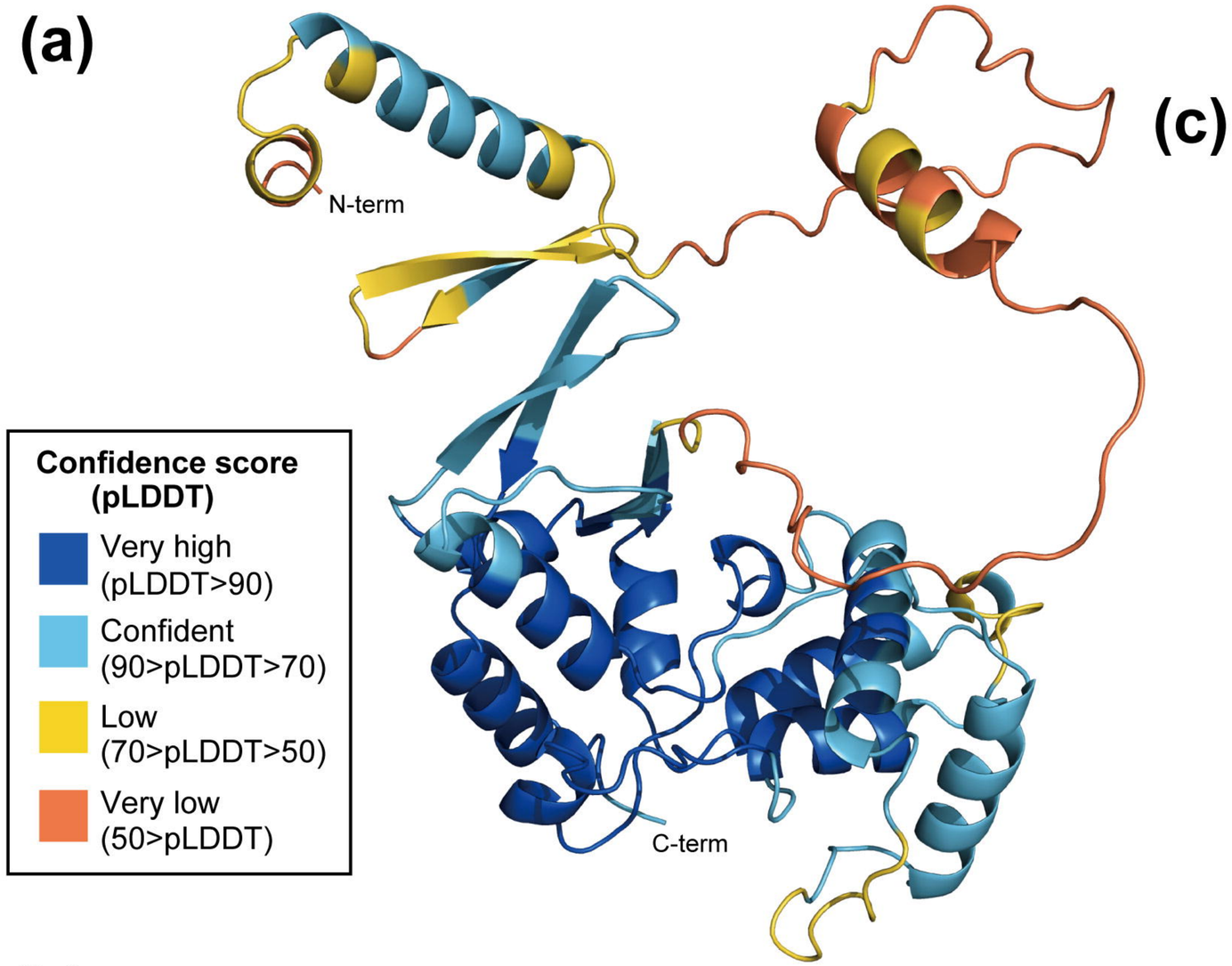
N-term
C-term
Confidence score (pLDDT)
Very high (pLDDT>90)
Confident (90>pLDDT>70)
Low (70>pLDDT>50)
Very low (50>pLDDT)

(c)

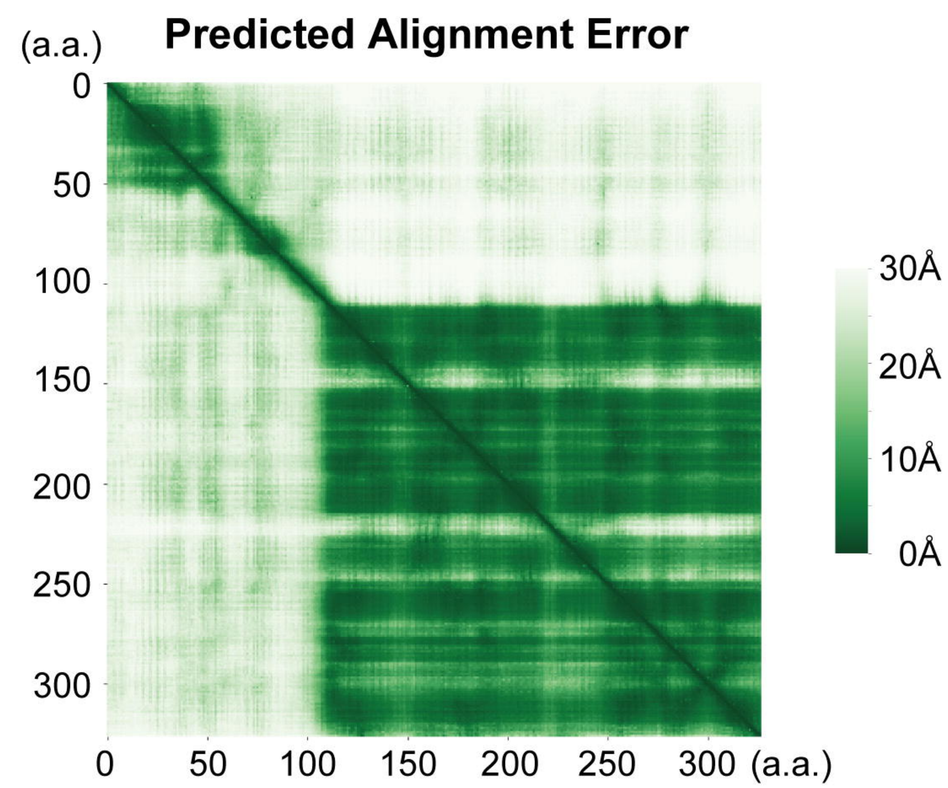
Predicted Alignment Error
(a.a.)
0
50
100
150
200
250
300
(a.a.)
30Å
20Å
10Å
0Å

(b)

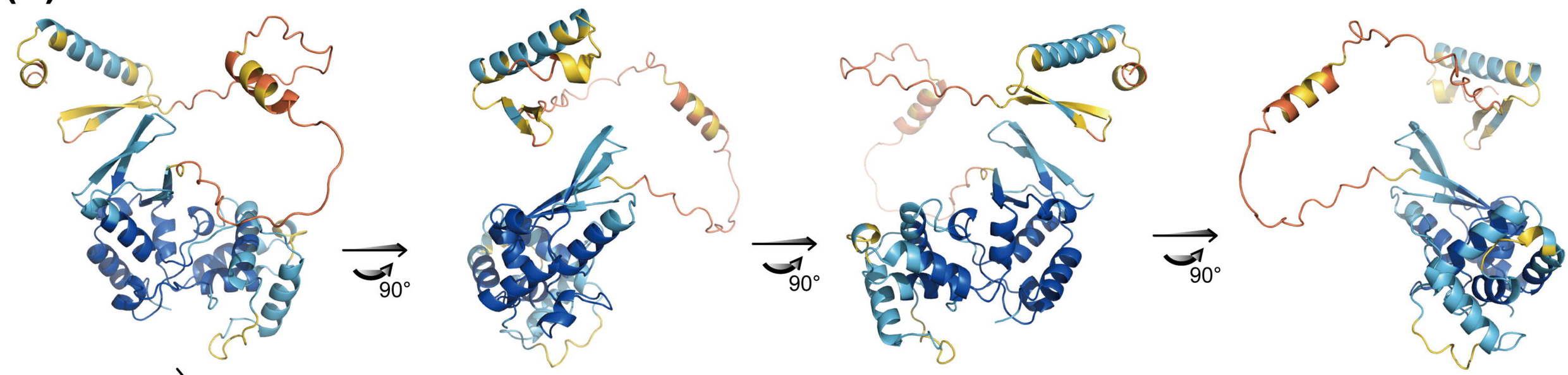
90°
90°
90°

Fig.2

(a)

```
KSHV_ORF34   0   ------------------------------------------------------------------------------------ 0
MHV68_ORF34  0   ------------------------------------------------------------------------------------ 0
EBV_BGLF3    0   ------------------------------------------------------------------------------------ 0
HCMV_UL95    60  MMAAAVVRAEVRRQRREERKKMAAARTTEDPPENHVVADVACGTGAVTRSSSSSLVVSSS 60
HHV6B_U67    0   ------------------------------------------------------------------------------------ 0

KSHV_ORF34   1   ------------------------------------------------------------MFALSSLVSEGDP---EV 15
MHV68_ORF34  1   ------------------------------------------------------------MATLSDFFPEADP---VL 15
EBV_BGLF3    1   ------------------------------------------------------------MFNAVKADMPDDP---ML 15
HCMV_UL95    61  SASGSDEPSSASPLSFPVCSPSTAVRSPGSAGVSTSLCSVERMVELS-AQSPAADFSVSE 120
HHV6B_U67    1   ---------------------------------------------MWVMSQVRSMEPDLTLAAVYQAAANLTEQD 30

                                                 E41A/T42A   F47A V50A
KSHV_ORF34   16  TSRYVKGVQLALDLSENT--PGQFKLIETPLNSFLLVSNVMPEVQPIC-SGRP---AL-- 67
MHV68_ORF34  16  EKNYRRCVDLAINMSWSV--PGQFKLVETPINSFLLVGDVLPNDMI---ESKP---VN-- 65
EBV_BGLF3    16  ARRYGQCLELALEACQDT--PEQFKLVETPLKSFLLVSNILPQDNRPWHEARS---SGRV 70
HCMV_UL95    121 AWRFEEAVNMALVACEAVSPYDRFRLIETPDENFLLVTNVIPRESAEVPVLDSSSSGGDS 180
HHV6B_U67    31  KEIFSEAVKTAFSVCSSAAPSARLRMIETPTQNFMFVTSVIPSGVPS-------------- 77

KSHV_ORF34   68  ---RPDFSNLHLPRL-------------------E----K-----LQRVLGQGFGAAGEE- 96
MHV68_ORF34  66  ---STNLVNIPFPLS-------------------T----LGVSTSKKSVEVTSYKSETEK- 99
EBV_BGLF3    71  AEDDYDFSSLALELL-------------------P----LNPRL----PEEWQFGGQGWS- 103
HCMV_UL95    181 GPEDK-KKNVGNKTAGEKNGGGSRAKRRRRRRAPKNDAATPSFLRRHDVLERFAAAAEPL 239
HHV6B_U67    78  GEKKT-KLNIDAAL---D-------------------NLALSF---------------ANKK 101

KSHV_ORF34   97  ----------IALDPSHVETHEKGQVFYNHYATEEWTWALTLNKDALLREAVDGLCDPGTW 147
MHV68_ORF34  100 ----------FQEAASISEHSIRGSIV---YEGLTWITAMGYNVTDFLVNMLEQMKCPENW 147
EBV_BGLF3    104 ----------SRMEPSQPE--MGMGLCFEVFDGDLMRIALAWNKDEVIGQALQILAHSQTW 152
HCMV_UL95    240 PSLCVRDYALRNADRVTYDGELIYGSYLLYRKAHVELSLSSNKVQHVEAVLRQVYTPGLL 299
HHV6B_U67    102 SKKMARTYLLQNVSRTQDQQVAISGTYILYTKKHIETSLMLDKTKLVKQILEYAETPNLL 161

                 D154A   W160A  G165A  S168A  C170A  C175A   G182A   L188A/L189A Y194A
KSHV_ORF34   148 KGLLPDDPLPLLWLLFNGPASFCRADCCLYKQHCG--YPGPVLLPGHMYAPKRDLLSFVN 205
MHV68_ORF34  148 SGLHPVDPLACVWLLYFGPKSRCSEIACVSELFIG--KKGPILLPPHMYRGDTSVNSFAH 205
EBV_BGLF3    153 TSLVPEDPLPWMWALFYGPRSHCEERHCVYAAARG--KRGPILLPTAVYTPCANIEAFLA 210
HCMV_UL95    300 DHHNVCDVEALLWLLYCGPRSFCARDTCFGREKNG--CPFPALLPKLFYEPVRDYMTYMN 357
HHV6B_U67    162 GYTDVRDLECLLWLVFCGPKSFCQSDSCFGYSKTGYNAAFPNLLPPYLYECGQNNGLFFG 201

                 Y215A
KSHV_ORF34   206 HALKYTKFLYGDFSGTWAAAC-------------R-----------------------PP 229
MHV68_ORF34  206 HLCQYVKHLYADYEPEIL-----------------S-----------------------CP 226
EBV_BGLF3    211 HLTRCVYALYLDVRDWKGEDI---------------A-----------------------PP 234
HCMV_UL95    358 LAELYVFVWYRGYEFPAPTPQATTAGSGGGGGAGACAVETSASAGRVDDAGDEVHLPLKP 417
HHV6B_U67    202 IVQAYVFSWYSDFDFSALEIS-------------------------------------E 223

                 R234A                                C256A   C259A   Q264A/N265A
KSHV_ORF34   230 FATSRIQRVVSQMKIIDA-----SDTYISHTCLLCHIYQQNSI--I--AG--QGTHVGGI 278
MHV68_ORF34  227 LDITRVKGCLSDLRQVAE-----SCVFLSQRCLLCHLYKQNAA--V--SK--NILTASDC 275
EBV_BGLF3    235 FDVSRLNKMAKQLCLLPQ-----EPFCITRVCLLCLLHKQNLNAQY--KR--PVDTYDPC 285
HCMV_UL95    418 VSLDRLREVLQAVRGRFSGREVPAWPASSRTCLLCALYSQNRLCLDLARDEARTVSYSPI 477
HHV6B_U67    224 RARRRIRSLLYDLKQKFSEQEISVLPVASQMCIFCALYKQNKLSLEYVSGDLKTSVFSPI 283

                                                 Y310A
KSHV_ORF34   279 LLLSGKGTQYITGNVQTQRCPTTGDYLIIPSYDIPAIITMIKENGLNQL-------- 327
MHV68_ORF34  276 IILGGSGKSLLGTYMKSYKDPATHDSILLPTYNLEAIVNYILEHYGHETAGQEINWE 332
EBV_BGLF3    286 LILTGEAERYMVDAVGNYREASTGTTVLYPTYDLGSIVADMVTYEDE---------- 332
HCMV_UL95    478 VIQDC--AAAVTDVTLSHILPGQSTVSLFPVYHVGKLLDALSLNDAGLITLNL---- 528
HHV6B_U67    284 IIKDC--LCVQTTISTTQMLPGTKSSAIFPVYDLRKLLSALVISEGSV-RFDI---- 333
```

(b)

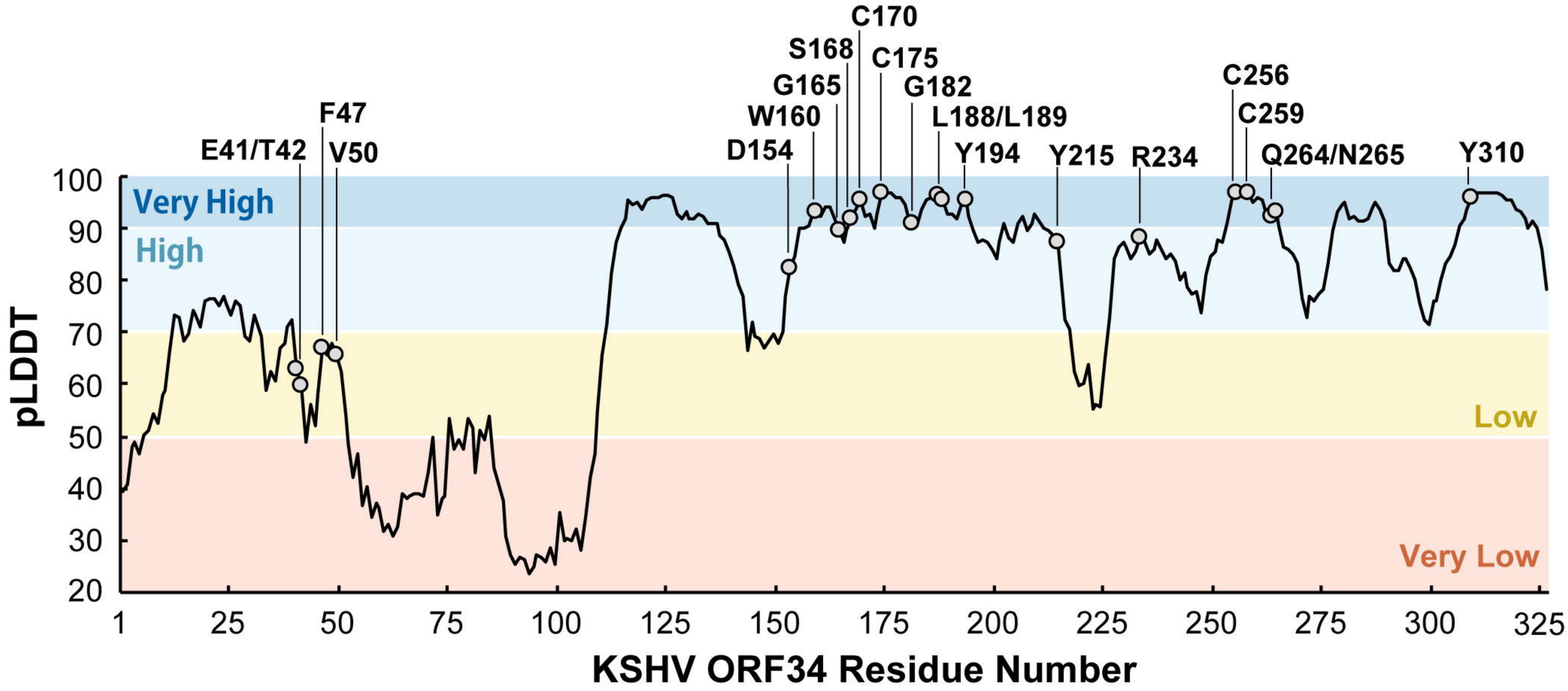

Fig.3

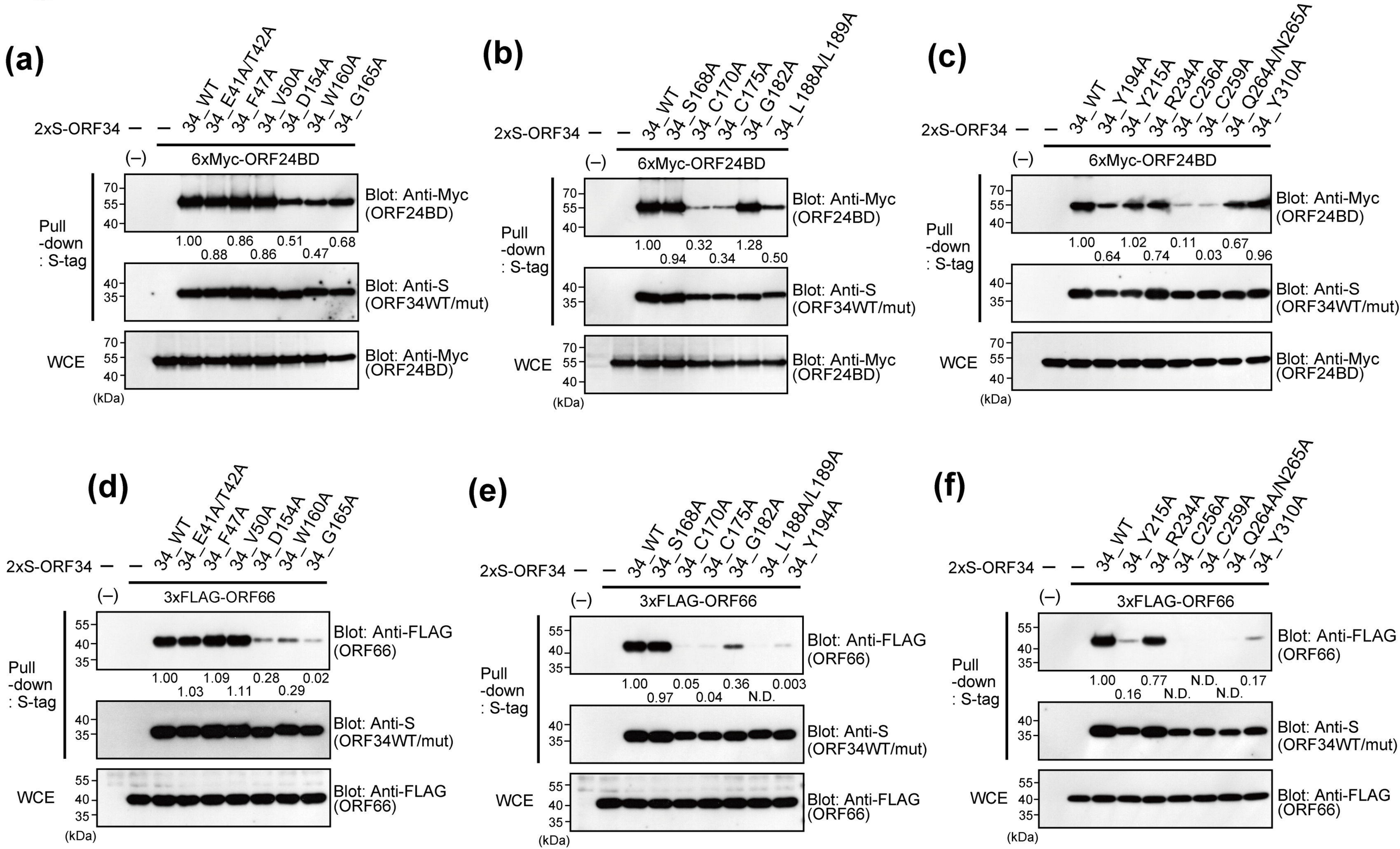
(a)
2xS-ORF34
34_WT
34_E41A/T42A
34_F47A
34_V50A
34_D154A
34_W160A
34_G165A
(–)
6xMyc-ORF24BD
Pull-down : S-tag
Blot: Anti-Myc (ORF24BD)
1.00 0.86 0.51 0.68
0.88 0.86 0.47
Blot: Anti-S (ORF34WT/mut)
WCE
Blot: Anti-Myc (ORF24BD)
(kDa)
(b)
2xS-ORF34
34_WT
34_S168A
34_C170A
34_C175A
34_G182A
34_L188A/L189A
(–)
6xMyc-ORF24BD
Pull-down : S-tag
Blot: Anti-Myc (ORF24BD)
1.00 0.32 1.28
0.94 0.34 0.50
Blot: Anti-S (ORF34WT/mut)
WCE
Blot: Anti-Myc (ORF24BD)
(kDa)
(c)
2xS-ORF34
34_WT
34_Y194A
34_Y215A
34_R234A
34_C256A
34_C259A
34_Q264A/N265A
34_Y310A
(–)
6xMyc-ORF24BD
Pull-down : S-tag
Blot: Anti-Myc (ORF24BD)
1.00 1.02 0.11 0.67
0.64 0.74 0.03 0.96
Blot: Anti-S (ORF34WT/mut)
WCE
Blot: Anti-Myc (ORF24BD)
(kDa)
(d)
2xS-ORF34
34_WT
34_E41A/T42A
34_F47A
34_V50A
34_D154A
34_W160A
34_G165A
(–)
3xFLAG-ORF66
Pull-down : S-tag
Blot: Anti-FLAG (ORF66)
1.00 1.09 0.28 0.02
1.03 1.11 0.29
Blot: Anti-S (ORF34WT/mut)
WCE
Blot: Anti-FLAG (ORF66)
(kDa)
(e)
2xS-ORF34
34_WT
34_S168A
34_C170A
34_C175A
34_G182A
34_L188A/L189A
34_Y194A
(–)
3xFLAG-ORF66
Pull-down : S-tag
Blot: Anti-FLAG (ORF66)
1.00 0.05 0.36 0.003
0.97 0.04 N.D.
Blot: Anti-S (ORF34WT/mut)
WCE
Blot: Anti-FLAG (ORF66)
(kDa)
(f)
2xS-ORF34
34_WT
34_Y215A
34_R234A
34_C256A
34_C259A
34_Q264A/N265A
34_Y310A
(–)
3xFLAG-ORF66
Pull-down : S-tag
Blot: Anti-FLAG (ORF66)
1.00 0.77 N.D. 0.17
0.16 N.D. N.D.
Blot: Anti-S (ORF34WT/mut)
WCE
Blot: Anti-FLAG (ORF66)
(kDa)

Fig.4

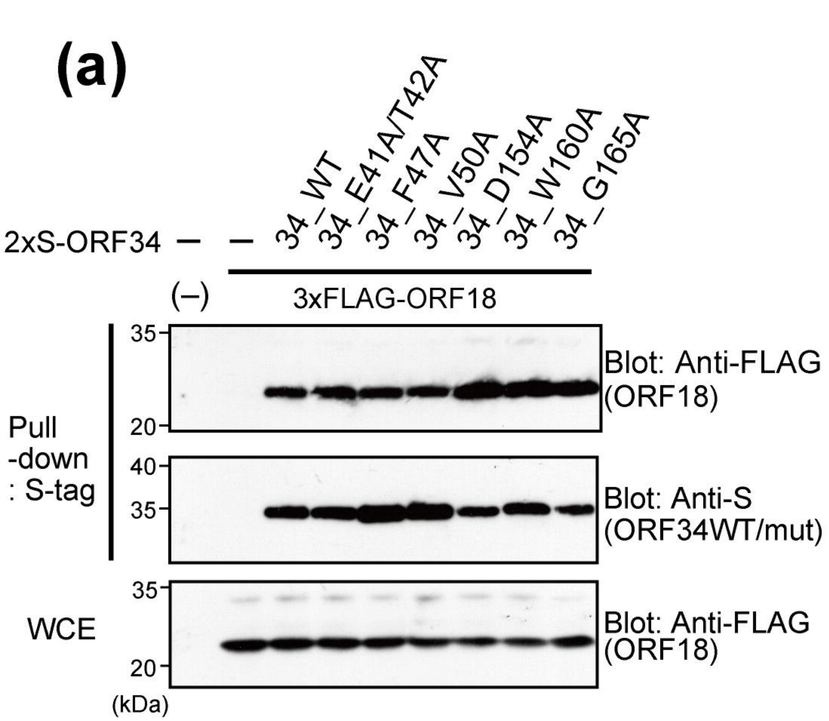
(a)
34_WT
34_E41A/T42A
34_F47A
34_V50A
34_D154A
34_W160A
34_G165A
2xS-ORF34
(–)
3xFLAG-ORF18
Pull-down : S-tag
WCE
Blot: Anti-FLAG (ORF18)
Blot: Anti-S (ORF34WT/mut)
Blot: Anti-FLAG (ORF18)
35
20
40
35
35
20
(kDa)

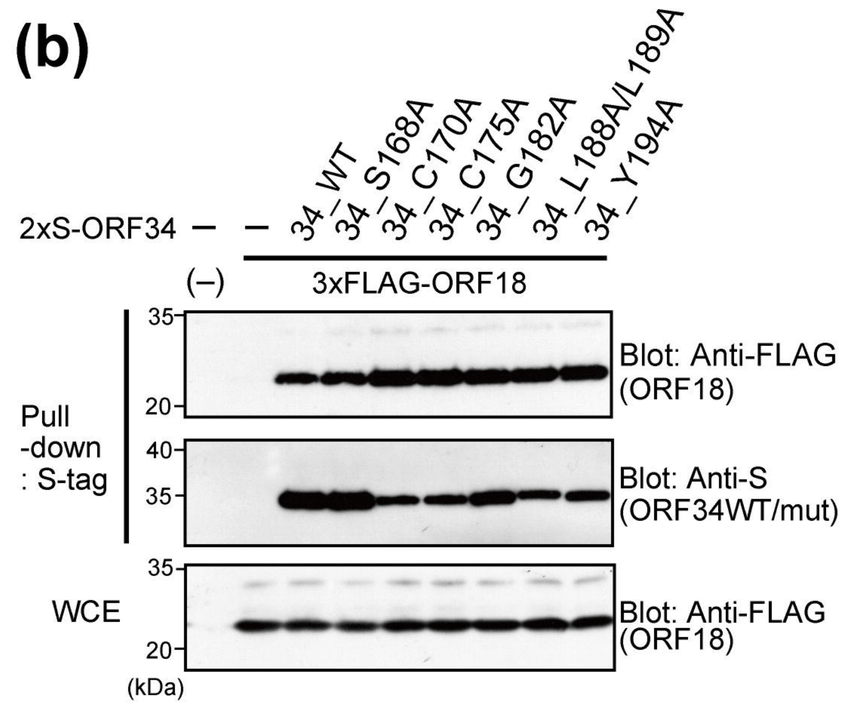
(b)
34_WT
34_S168A
34_C170A
34_C175A
34_G182A
34_L188A/L189A
34_Y194A
2xS-ORF34
(–)
3xFLAG-ORF18
Pull-down : S-tag
WCE
Blot: Anti-FLAG (ORF18)
Blot: Anti-S (ORF34WT/mut)
Blot: Anti-FLAG (ORF18)
35
20
40
35
35
20
(kDa)

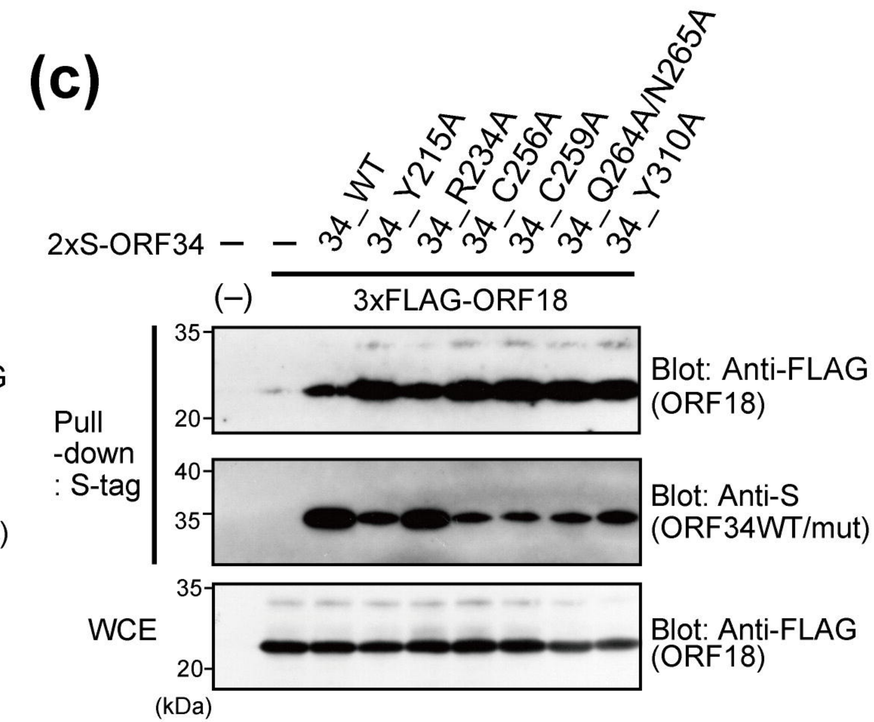
(c)
34_WT
34_Y215A
34_R234A
34_C256A
34_C259A
34_Q264A/N265A
34_Y310A
2xS-ORF34
(–)
3xFLAG-ORF18
Pull-down : S-tag
WCE
Blot: Anti-FLAG (ORF18)
Blot: Anti-S (ORF34WT/mut)
Blot: Anti-FLAG (ORF18)
35
20
40
35
35
20
(kDa)

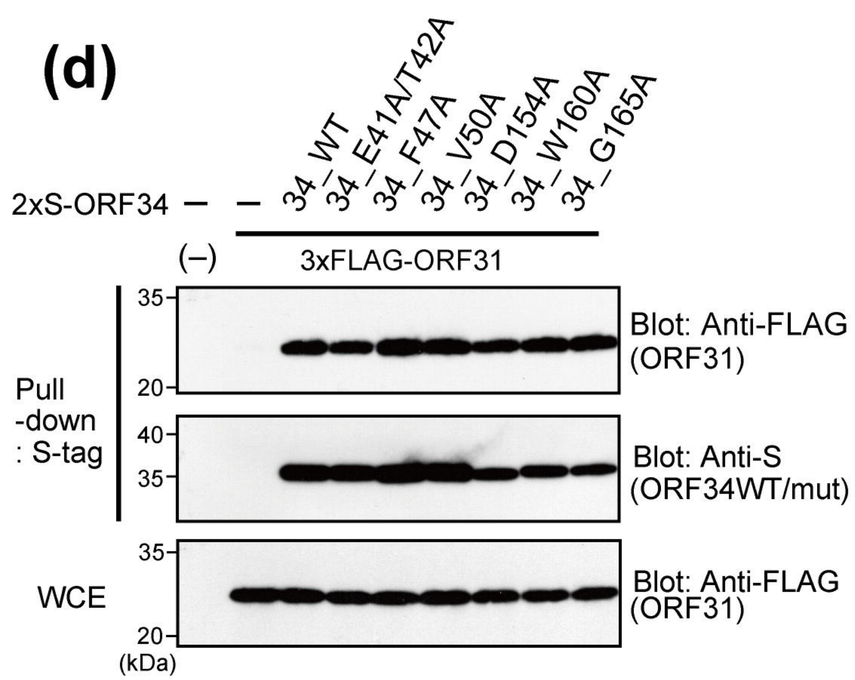
(d)
34_WT
34_E41A/T42A
34_F47A
34_V50A
34_D154A
34_W160A
34_G165A
2xS-ORF34
(–)
3xFLAG-ORF31
Pull-down : S-tag
WCE
Blot: Anti-FLAG (ORF31)
Blot: Anti-S (ORF34WT/mut)
Blot: Anti-FLAG (ORF31)
35
20
40
35
35
20
(kDa)

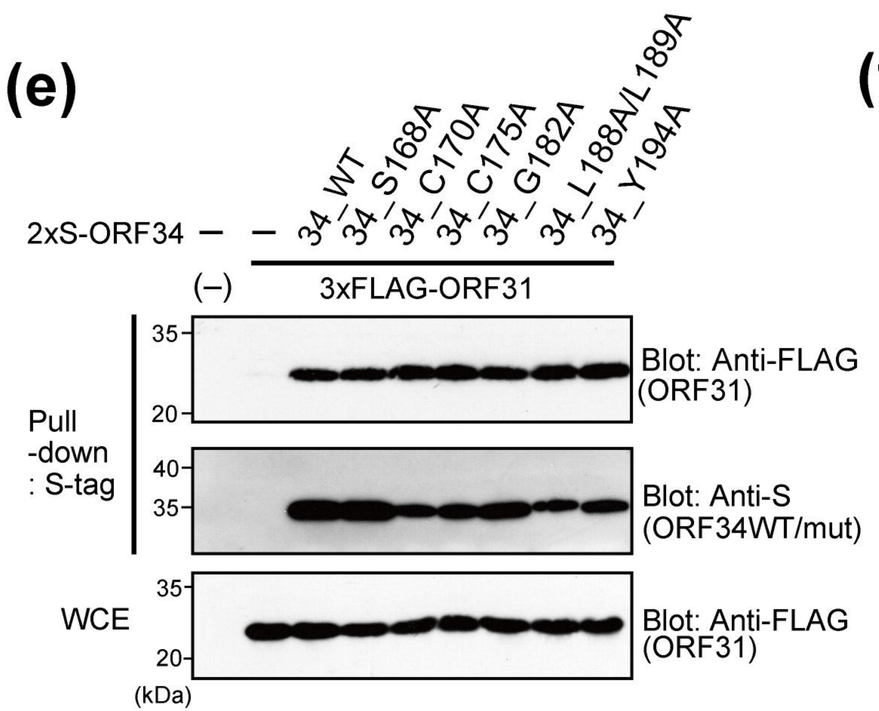
(e)
34_WT
34_S168A
34_C170A
34_C175A
34_G182A
34_L188A/L189A
34_Y194A
2xS-ORF34
(–)
3xFLAG-ORF31
Pull-down : S-tag
WCE
Blot: Anti-FLAG (ORF31)
Blot: Anti-S (ORF34WT/mut)
Blot: Anti-FLAG (ORF31)
35
20
40
35
35
20
(kDa)

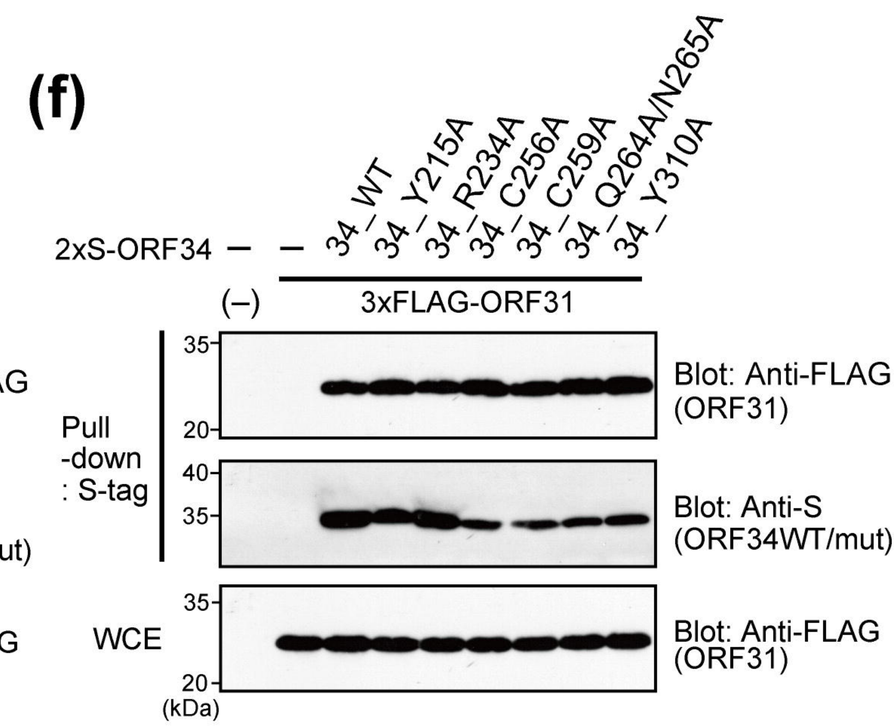
(f)
34_WT
34_Y215A
34_R234A
34_C256A
34_C259A
34_Q264A/N265A
34_Y310A
2xS-ORF34
(–)
3xFLAG-ORF31
Pull-down : S-tag
WCE
Blot: Anti-FLAG (ORF31)
Blot: Anti-S (ORF34WT/mut)
Blot: Anti-FLAG (ORF31)
35
20
40
35
35
20
(kDa)

WBtiff->120%

Fig.5

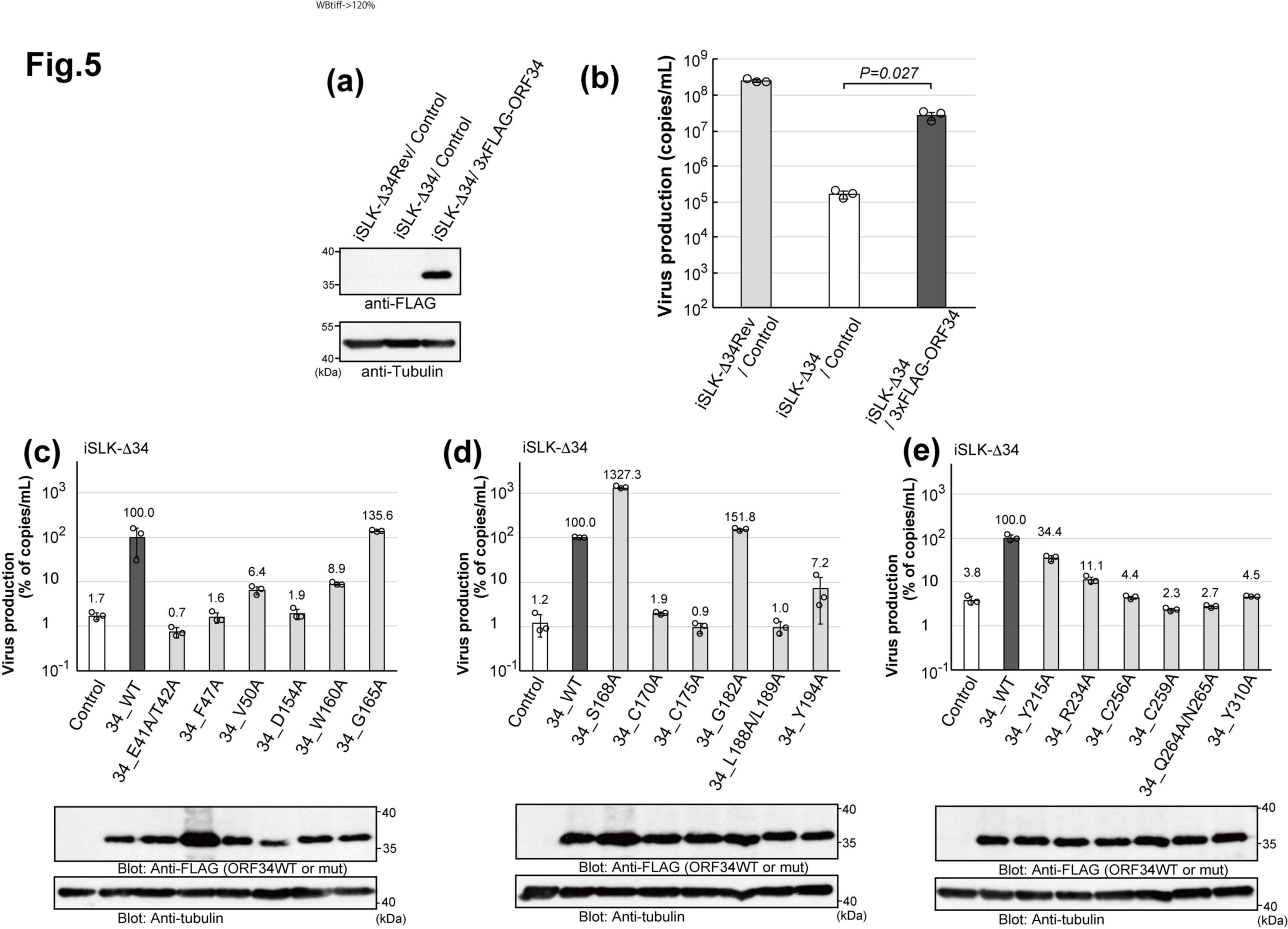

Fig.6

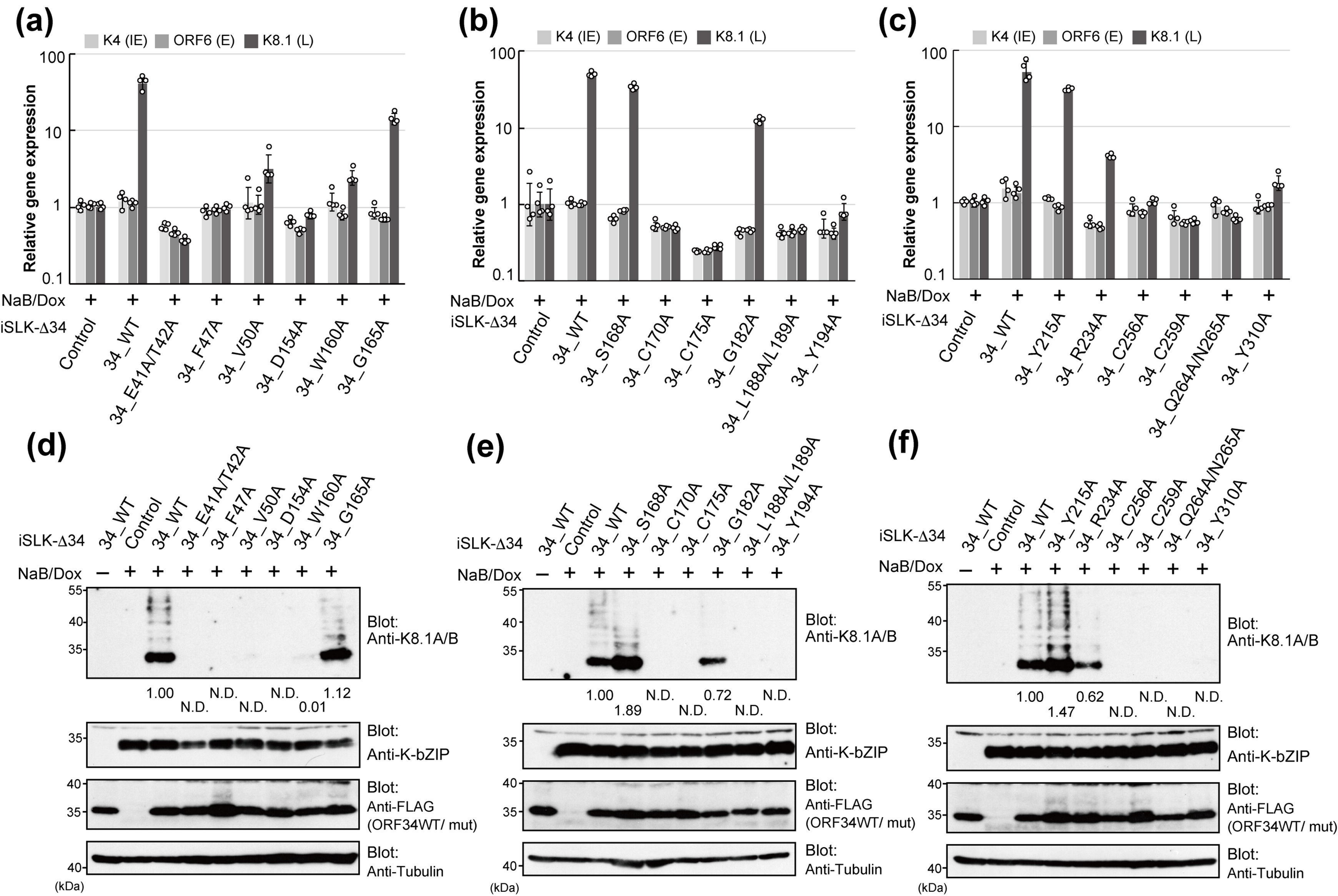
(a)
K4 (IE)
ORF6 (E)
K8.1 (L)
Relative gene expression
100
10
1
0.1
NaB/Dox
iSLK-Δ34
Control
34_WT
34_E41A/T42A
34_F47A
34_V50A
34_D154A
34_W160A
34_G165A
(b)
34_S168A
34_C170A
34_C175A
34_G182A
34_L188A/L189A
34_Y194A
(c)
34_Y215A
34_R234A
34_C256A
34_C259A
34_Q264A/N265A
34_Y310A
(d)
Blot:
Anti-K8.1A/B
1.00
N.D.
N.D.
1.12
N.D.
N.D.
0.01
Blot:
Anti-K-bZIP
Blot:
Anti-FLAG
(ORF34WT/ mut)
Blot:
Anti-Tubulin
(kDa)
55
40
35
(e)
1.00
N.D.
0.72
N.D.
1.89
N.D.
N.D.
(f)
1.00
0.62
N.D.
N.D.
1.47
N.D.
N.D.

Fig.7

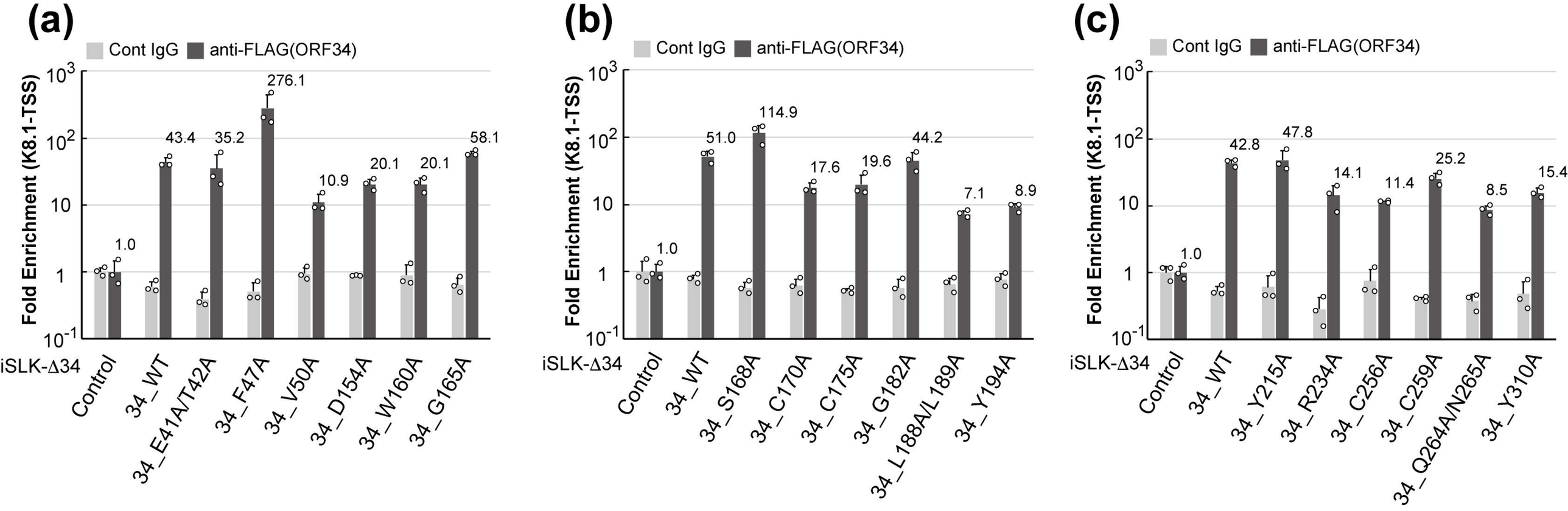
(a)
Cont IgG
anti-FLAG(ORF34)
Fold Enrichment (K8.1-TSS)
10^3
10^2
10
1
10^{-1}
1.0
43.4
35.2
276.1
10.9
20.1
20.1
58.1
iSLK-Δ34
Control
34_WT
34_E41A/T42A
34_F47A
34_V50A
34_D154A
34_W160A
34_G165A
(b)
Cont IgG
anti-FLAG(ORF34)
Fold Enrichment (K8.1-TSS)
1.0
51.0
114.9
17.6
19.6
44.2
7.1
8.9
iSLK-Δ34
Control
34_WT
34_S168A
34_C170A
34_C175A
34_G182A
34_L188A/L189A
34_Y194A
(c)
Cont IgG
anti-FLAG(ORF34)
Fold Enrichment (K8.1-TSS)
1.0
42.8
47.8
14.1
11.4
25.2
8.5
15.4
iSLK-Δ34
Control
34_WT
34_Y215A
34_R234A
34_C256A
34_C259A
34_Q264A/N265A
34_Y310A

Fig.8

(a)

	ORF34 WT/mutant	Virus production	K8.1 protein	K8.1-TSS recruitment	K8.1 mRNA	ORF24BD binding	ORF66 binding
Group 1	Y215A	0.344	1.477	1.116	0.572	1.023	0.167
	WT	1.000	1.000	1.000	1.000	1.000	1.000
	G182A	1.518	0.725	0.866	0.250	1.286	0.359
	G165A	1.356	1.128	1.340	0.343	0.680	0.022
Group 2	Q264A_N265A	0.027	N.D.	0.199	0.011	0.665	N.D.
	Y194A	0.072	N.D.	0.175	0.017	0.645	0.003
	L188A_L189A	0.010	N.D.	0.140	0.009	0.503	N.D.
	W160A	0.089	0.013	0.465	0.059	0.473	0.289
	D154A	0.019	N.D.	0.463	0.019	0.512	0.282
	Y310A	0.045	N.D.	0.359	0.035	0.956	0.173
Group 3	C175A	0.009	N.D.	0.385	0.006	0.345	0.039
	C170A	0.019	N.D.	0.345	0.010	0.325	0.057
	C256A	0.044	N.D.	0.265	0.020	0.109	N.D.
	C259A	0.023	N.D.	0.589	0.011	0.027	N.D.
Group 4	R234A	0.111	0.626	0.329	0.077	0.740	0.775
	V50A	0.064	N.D.	0.252	0.077	0.861	1.114
	E41A_T42A	0.007	N.D.	0.812	0.009	0.877	1.033
	F47A	0.016	N.D.	6.367	0.023	0.859	1.086
	S168A	13.273	1.889	2.252	0.679	0.940	0.969

N.D.
(Not detected)

0 1 2 3
(ORF34 WT as 1.0)

(b)

Relative SASA	ORF34 Resudues
0.00	Y215
0.64	G182
0.00	G165
0.02/0.13	Q264_N265
0.02	Y194
0.07/0.02	L188_L189
0.07	W160
0.09	D154
0.01	Y310
0.01	C175
0.06	C170
0.00	C256
0.04	C259
0.29	R234
0.41	V50
0.63/0.17	E41_T42
0.19	F47
0.01	S168

(>0.1: estimated to be surface exposed)

Fig. 9

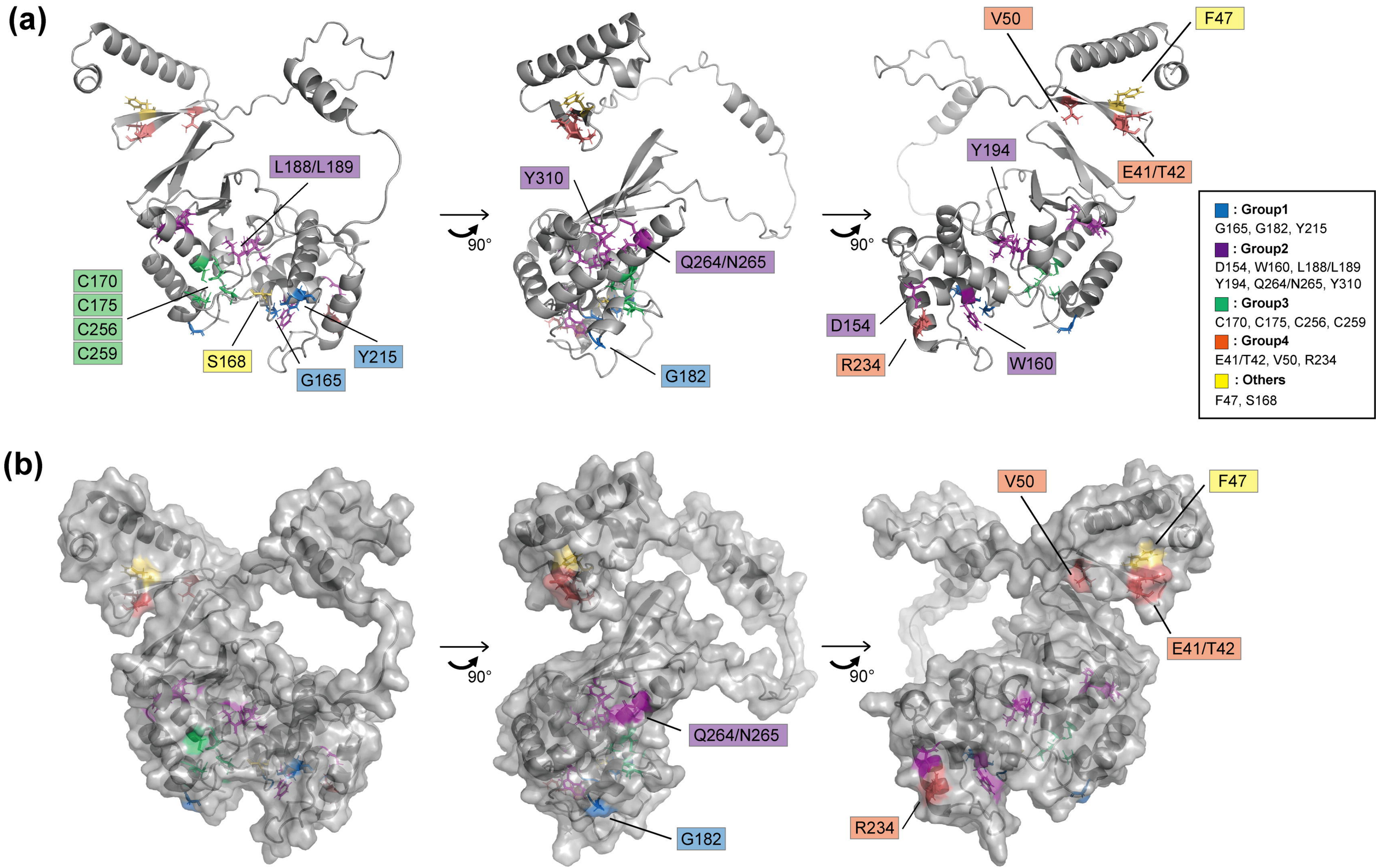
(a)
L188/L189
C170
C175
C256
C259
S168
G165
Y215
90°
Y310
Q264/N265
G182
90°
V50
F47
Y194
E41/T42
D154
R234
W160
: Group1
G165, G182, Y215
: Group2
D154, W160, L188/L189
Y194, Q264/N265, Y310
: Group3
C170, C175, C256, C259
: Group4
E41/T42, V50, R234
: Others
F47, S168
(b)
90°
Q264/N265
G182
90°
V50
F47
E41/T42
R234

Fig.10

(a)

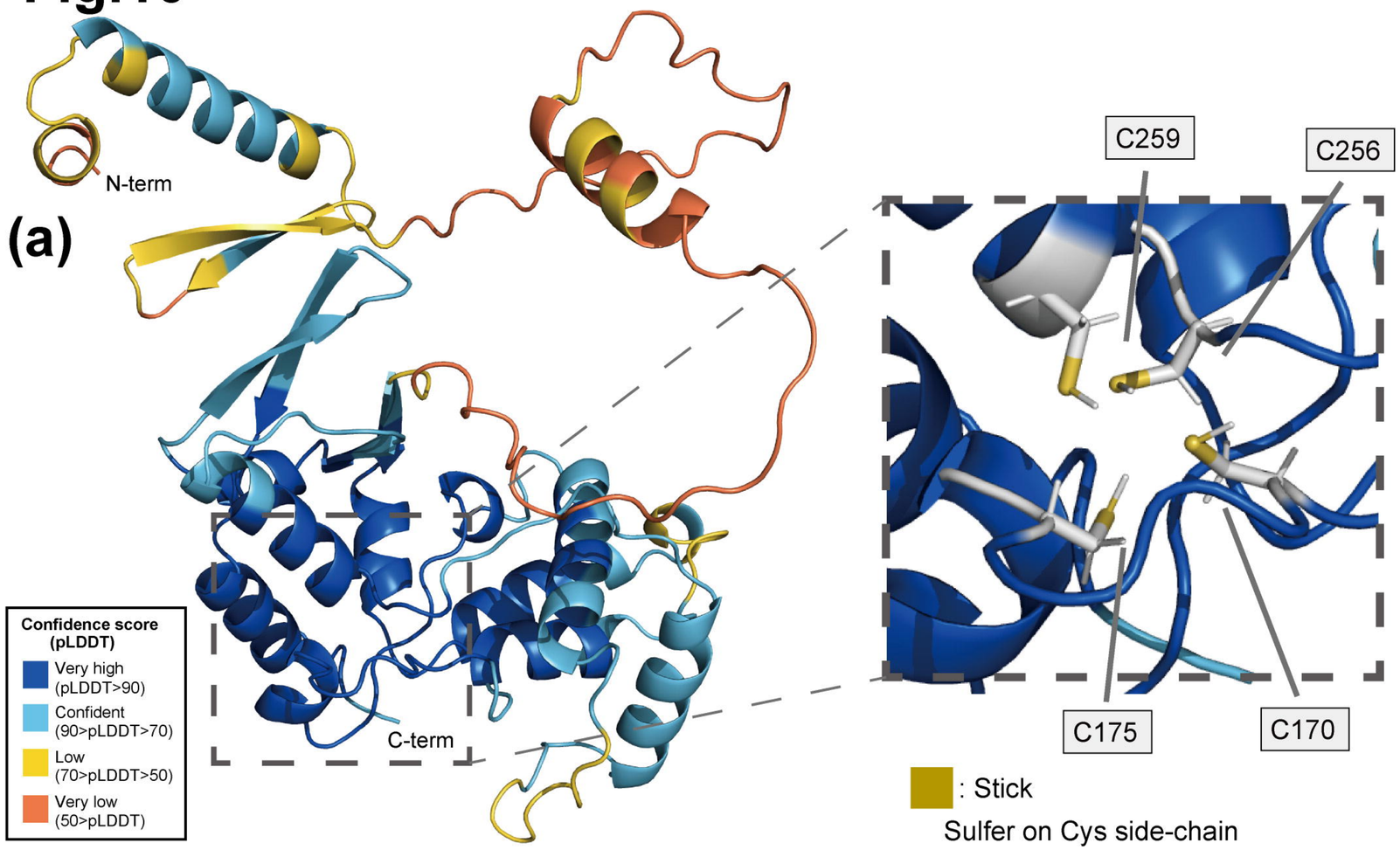

(b)

Binding ion	Binding residues	Template	Score
Cu^{+}	256C, 259C	5vdf_A0	6.519
Zn^{2+}	170C, 175C, 256C, 259C	5xfp_B0	5.468
Fe^{3+}	170C, 175C, 256C, 259C	3lmc_A0	5.272
Fe^{2+}	170C, 175C, 256C, 259C	5v27_A1	3.996
Pb^{2+}	175C, 255T, 256C, 259C	1iw7_D1	3.779
Cd^{2+}	256C, 259C	1fe0_A0	3.658
Cd^{2+}	255T, 256C, 259C	3cjk_B0	3.655
Zn^{2+}	170C, 177Y, 256C, 259C	4c4a_A0	3.394
Zn^{2+}	170C, 175C, 256C	5obz_B0	3.325
Hg^{2+}	170C, 175C, 176L, 256C	1r0g_A0	3.299
Fe^{2+}	170C, 175C, 177Y, 256C	5v27_A1	3.171
Zn^{2+}	256C, 259C	4a46_C0	3.087
Hg^{2+}	256C, 259C	1l8d_A0	3.082
Zn^{2+}	170C, 175C, 177Y, 256C	4mvt_B0	3.053

(c)

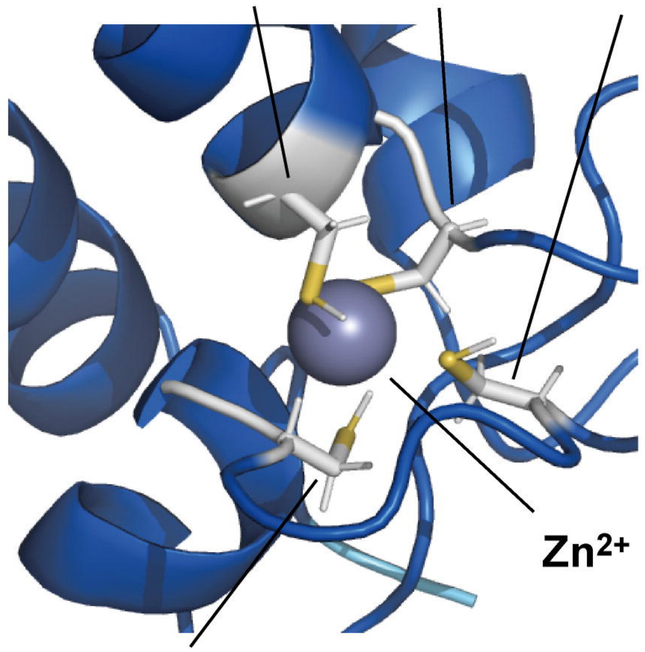

(d)

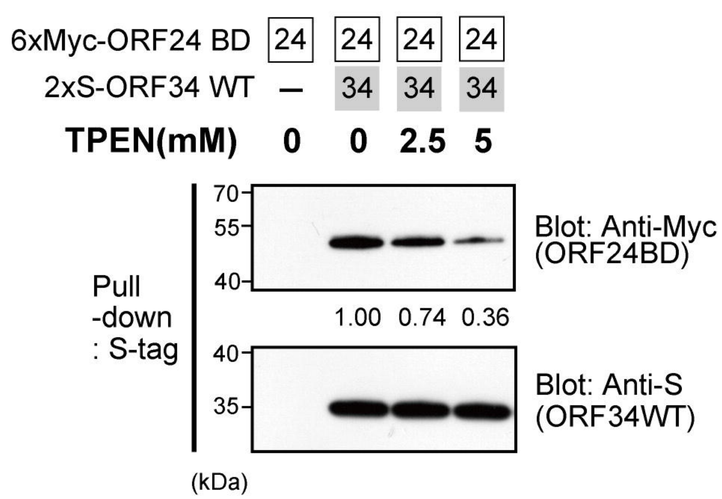
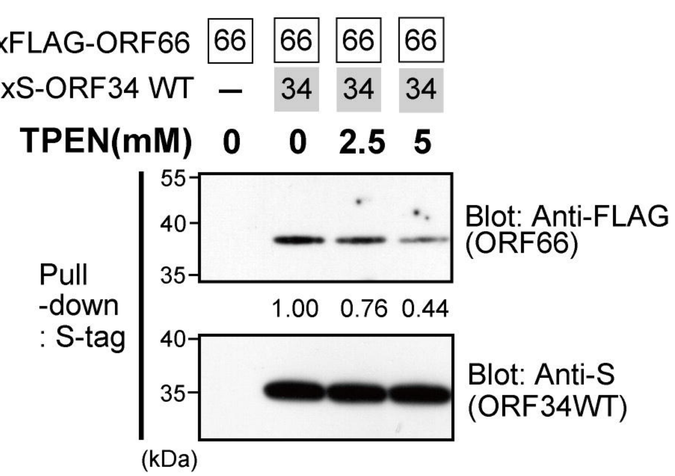
(e)